Journal of Elasticity
https://doi.org/10.1007/s10659-023-10028-7

RESEARCH

Anisotropy and Asymmetry of the Elastic Tensor of Lattice Materials

Huiming Yin[1] · **Chao Liu**[1]

Received: 31 December 2022 / Accepted: 1 July 2023

Abstract
Lattice materials formed by hinged springs or linear elastic bonds may exhibit diverse anisotropy and asymmetry features of the overall elastic behavior depending on their unit cell configuration. The recently developed singum model transfers the force-displacement relationship of the springs in the lattice to the stress-strain relationship in the continuum particle, and provides the analytical form of tangential elasticity. When a pre-stress exists in the lattice, the stiffness tensor significantly changes due to the effect of the configurational stress; existing methods like the lattice spring method, relying on a scalar energy equivalence, are insufficient in such situations. Instead, a tensorial homogenization method with the new definition of singum stress and strain, should be preferred. Different lattice structures lead to different symmetries of the stiffness tensors, which are demonstrated by five lattices. When all bonds exhibit the same length, regular hexagonal, honeycomb, and auxetic lattices demonstrate that the stiffness changes from an isotropic to anisotropic, from symmetric to asymmetric tensor. When the central symmetry of the unit cell is not satisfied, the primitive cell will contain more than one singums and the Cauchy–Born rule fails by the loss of equilibrium of the single singum. A secondary stress is induced to balance the singums. Displacement gradient $d_{ij} = u_{j,i}$ is proposed to replace strain in the constitutive law for the general case because d_{12} and d_{21} can produce different stress states. Although the hexagonal and honeycomb lattices may exhibit isotropic behavior, for general auxetic lattices, an anisotropic and asymmetric elastic tensor is obtained with the loss of both minor and major symmetry, which is also demonstrated in a square lattice with unbalanced central symmetry and a chiral lattice. The modeling procedure and results can be generalized to three dimensions and other lattices with the anisotropic and asymmetric stiffness.

Keywords Elasticity · Lattice materials · Singum model · Cauchy–Born rule · Stress and strain

Mathematics Subject Classification 74B10 · 74B20 · 74Q15

✉ H. Yin
yin@civil.columbia.edu

[1] Department of Civil Engineering and Engineering Mechanics, Columbia University, 610 Seeley W. Mudd 500 West 120th Street, New York, 10027, USA

Published online: 18 July 2023

1 Introduction

Classical elasticity under the linear infinitesimal deformation considers that the stress and strain are symmetric tensors with 3 or 6 independent components for 2D or 3D cases, respectively, in which the stiffness tensor correlates the strain to stress with the major and minor symmetries, i.e. $C_{ijkl} = C_{klij} = C_{jikl} = C_{ijlk}$, and exhibits up to 6 or 21 independent elastic constants for 2D or 3D, respectively [20, 35]. The stress and strain fields shall also satisfy the equilibrium, compatibility, and boundary conditions, which leads to various classical boundary value problems (BVPs), general elastic solutions, and fundamental solutions, depending on the symmetries of the elastic tensor [37]. For simplicity, the isotropic elastic tensor based on two elastic constants becomes a very common assumption for elastic problems.

The asymmetry of stress can be traced back to Cosserat theory with the concept of couple stresses in 1909 [5] and revisited by Mindlin [21, 23], Eringen [11, 12], Nowacki [26], and Lake [16] etc. However, the classical symmetric strain is used to describe the deformation together with micro-rotation and curvature, which leads to a complex constitutive law of a Cosserat continuum with 903 elastic constants in the most general cases and 18 independent elastic constants for the isotropic case [22]. Although it can resolve some problems in classical elasticity, it creates difficulties on material characterization and determination of elastic constants.

With the emerging material process and characterization technologies, one can precisely control the microstructure through 3D design and printing, and observe some delicate lattice structures of natural materials. Various metamaterials and super lattices are observed or designed with versatile functions and unique material properties [3, 14, 33, 46], which classical elasticity cannot sufficiently explain [15, 24]. Because the force transfer through the lattices is through the network of the 1D bonds in the 2D or 3D spaces, the conventional micromechanics [25, 39] under the assumption of continuum cannot capture the discrete microstructure. Practically modeling lattice materials with appropriate stress-strain relationship is critical for the design and analysis of the relevant materials and structures.

The recently developed singum model [40, 41] uses the Wigner–Seitz (WS) cells of a lattice to represent a continuum solid. The stress and strain are defined by the force and displacement of the cutting points on the singum surfaces, so that the singular forces along the bonds in the continuous space can be transformed into the contacting stress between the continuum particles, namely singums, and the elastic tensor can be derived by applying a displacement variation through the Cauchy–Born rule [34, 40], which applies well to the central symmetry lattices. This paper derives the effective elasticity by a displacement controlled load. The Cauchy–Born rule has been widely used to relate macroscopic deformation of crystals to the changes in the lattice through an affine transformation [10] and will be used to relate the displacement field with the strain or displacement gradient.

Although most lattices exhibit anisotropic elastic behavior, a two-dimensional (2D) hexagonal lattice provides an isotropic elastic tensor in plane stress condition with a Poisson's ratio $\nu = 1/3$ and in plane strain condition with $\nu = 1/4$ if no prestress exists. Otherwise, the Poisson's ratio reduces with the tensile prestress and increase with a compressive prestress [45].

When a lattice is not central symmetric, such as a honeycomb lattice [40], a problem of the loss of equilibrium of a singum was found in the recent work when the Cauchy–Born rule is applied [34, 41]. Because a primitive unit cell, which contains more than one singum, shall stay in equilibrium due to the periodicity, to correct the problem, a secondary force is superposed to the singums in the primitive unit cell without generating an overall strain, so that the equilibrium problem is corrected for the honeycomb lattice [41].

When it is applied to auxetic metamaterials with a negative Poisson's ratio for the overall materials [17, 29], one can find that a shear in horizontal or vertical direction, say $u_{1,2}$ or $u_{2,1}$ produces different stress states, which should always be the same for classical elasticity due to the minor symmetry of the elastic tensor. This discrepancy motivates this paper to systemically investigate the anisotropy and asymmetry of the elastic tensor of lattice materials through the singum model as a follow-up to the previous work [41]. Similarly, as seen in this paper, given one uniform displacement pattern by $u_{i,j}$ for a chiral lattice subsequently, the stress induced can be asymmetric as well as $\sigma_{12} \neq \sigma_{21}$. Therefore, an asymmetric stress and displacement gradient (DG) shall be used in the constitutive law, which are defined as the singum stress and strain to replace the symmetric stress and strain in classical elasticity. When a material satisfies central symmetry, such as square lattices and hexagonal lattices [45], the new constitutive law recovers the classical elasticity tensor with both major and minor symmetries. However, the most general case of the stiffness tensor between the asymmetric stress and strain will include 16 or 81 elastic constants for 2D and 3D, respectively, without the major and minor symmetry.

This paper first reviews the singum construction for a regular central symmetric hexagonal lattice containing elastic bonds [40, 45] and defines the singum stress and strain as the average Cauchy stress and displacement gradient of a singum through the force and displacement on its cutting points of the surface. By applying a displacement variation, the variations of the stress and strain can be obtained, which recovers the isotropic constitutive law for a regular hexagonal lattice with central symmetry.

When the lattice is not central symmetric, a honeycomb lattice is used to demonstrate the effective stiffness. Because the primitive cell contains two singums, the superposition principle is used to achieve the equilibrium of the singums given a displacement variation. The stress-strain relationship is obtained and the instability of the stiffness tensor is demonstrated [41].

When an auxetic lattice is used, the asymmetric stress is obtained for a displacement variation, which shows the necessity to replace the classical strain with DG in the constitutive law. An anisotropic stiffness tensor correlates the stress to strain without the minor or major symmetry. The similar phenomenon has also been observed in an unbalanced square lattice with central symmetry and a chiral lattice. The application of DG to the rigid body rotation is discussed for the application of the new constitutive relationship. The constitutive modeling with the singum model can be straightforwardly extended to the general 3D lattices.

The anisotropic, asymmetric constitutive law discloses the mechanics and physics of the effective material behavior of lattice-based solids in a clear way. Although most natural materials exhibit the symmetry and classical elasticity tensor can describe the elastic behavior sufficiently, for some unique lattice materials, such as auxetic lattices [41], chiral lattices [4, 33], and origami lattices [19], the anisotropy and asymmetry of the elastic tensor dominate and the present representation of the constitutive law with the singum model will be a useful tool. Its impacts to elastic boundary value problems are discussed and demonstrated. Particularly, the main difference is that $u_{i,j}$ and $u_{j,i}$ with $i \neq j$ may produce different stresses, while they commonly provide the same stress state in classical linear elasticity with the minor symmetry.

The remainder of the paper demonstrates the singum model through five lattices, namely, 1) a regular hexagonal lattice with central symmetry [45], 2) a regular honeycomb lattice [41], 3) an auxetic lattice [41], 4) an unbalanced square lattice with central symmetry, and 5) a chiral lattice, which show that the effective elastic tensor changes from isotropic to anisotropic, from symmetric to asymmetric. Note that the first three cases have been investigated in the recent papers [41, 45]. However, the conventional stress and strain were used

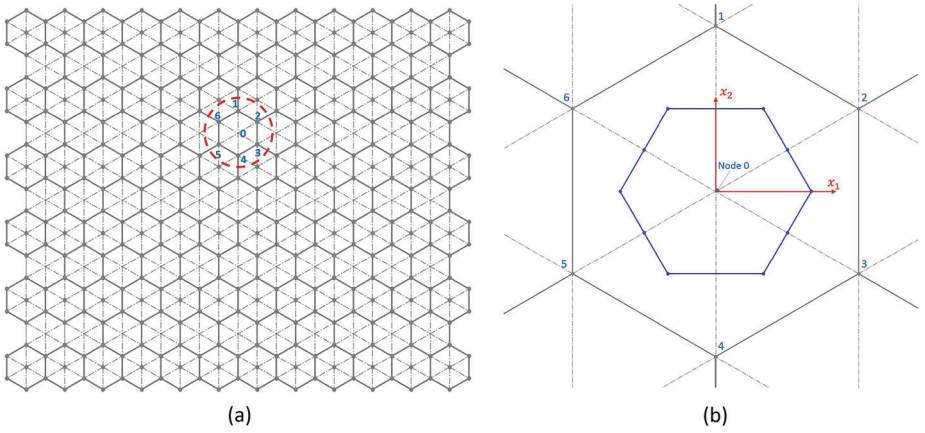

Fig. 1 The singum construction of a regular hexagonal lattice: (a) the regular hexagonal lattice with a representative node highlighted and (b) the singum particle of Node 0 as a primitive cell [44]

in the constitutive law, which exhibits a challenging problem for Case 3 that asymmetric stresses $\sigma_{12} \neq \sigma_{21}$ is yielded. Therefore, this paper will use the displacement gradient (DG) as the singum strain to replace the strain in the classical constitutive law. Although it produces the same stiffness tensor for the regular hexagonal lattice due to the central symmetry, it will resolve the dilemma that the classical elasticity tensor cannot describe some special lattices, such as the auxetic and chiral lattices, with the asymmetry of stress or strain, which will be elaborated subsequently. For general asymmetric elastic lattices, some remarks are provided, and future research following this work are briefly discussed.

2 Singum Model of a Regular Hexagonal Lattice with Central Symmetry

Following the previous papers [45], we first use a regular hexagonal lattice in a two-dimensional (2D) space to demonstrate the singum construction.

2.1 Singum Construction

In Fig. 1(a), the lattice consists of the same bonds or springs with length $2l_p^0$ and spring coefficient k, which form regular triangles. Therefore, each node connects to 6 neighbors forming a hexagon as the regular unit cell, which is highlighted by the red circle for Node 0. The singum of a node is constructed by cutting its neighboring bonds with the vertical mid-planes in 3D or mid-lines in 2D. Figure 1(b) shows the singum particle of Node 0 in 2D as a hexagon with the edge length of $\frac{2l_p^0}{\sqrt{3}}$, which is the Wigner–Seitz (WS) cell of the lattice [38].

A Cartesian coordinate $\mathbf{X}$ is set up at the initial state as the material coordinate, in which all bonds exhibit zero force and the total potential energy is zero. The spatial coordinate $\mathbf{x}$ is set up at the deformed state. Without any loss of generality, the origins of $\mathbf{x}$ and $\mathbf{X}$ are both selected at the center of Atom 0. The displacement field is written as $\mathbf{u} = \mathbf{x} - \mathbf{X}$. The deformation gradient tensor is defined as $F_{ik} = \frac{\partial x_i}{\partial X_k}$. The finite strain can be defined either in the Lagrangian coordinates as $E_{ij} = \frac{1}{2}(F_{ki}F_{kj} - \delta_{ij})$ or in the Eulerian coordinates

as $\varepsilon_{ij} = \frac{1}{2}(\delta_{ij} - F_{ki}^{-1}F_{kj}^{-1})$ [34, 42]. The stress and strain in this paper are measured in the spatial coordinate. We define the displacement gradient (DG) tensor as

$$d_{ij} = \frac{\partial u_j}{\partial x_i} = \delta_{ij} - F_{ij}^{-1}, \tag{1}$$

which defines the spatial strain in the Eulerian coordinate as:

$$\varepsilon_{ij} = \frac{1}{2}(d_{ij} + d_{ji} - d_{ki}d_{kj}). \tag{2}$$

Note that d_{ij} is asymmetric; while ε_{ij} is symmetric. The Cauchy stress σ_{ij} can be used in couple with them for the constitutive modeling. In classical linear elasticity, ε_{ij} is used with the symmetry, and the higher order term in Eq. (2) is negligible. However, this paper shows d_{ij} provides a more straightforward way to connect with Cauchy stress σ_{ij}, although it can be subsequently correlated to ε_{ij} by Eq. (2).

Here the indices of Cauchy stress tensor σ_{ij} follow the convention of a cubic element that the first index i indicates the surface and the second index j the direction of the stress vector on the surface. Therefore, on any surface with a directional n_i, the stress vector can be written as $t_j = n_i\sigma_{ij}$. The constitutive relation between σ_{ij} and d_{kl} in the linear deformation range is written as

$$\sigma_{ij} = C_{ijkl}d_{kl}, \tag{3}$$

where the stiffness tensor shares the same expression as classical elasticity if d_{kl} and d_{lk} always induce the same stress, which makes the minor symmetry of $C_{ijkl} = C_{jikl} = C_{ijlk}$. However, in general cases of lattice materials, when d_{kl} and d_{lk} induce different stress states, the minor symmetry will be lost; the major symmetry of $C_{ijkl} = C_{klij}$ will also be lost due to the lattice nature with the configurational stress, which will be discussed subsequently. Therefore, the stiffness tensor exhibits 81 independent constants as the maximum; whereas classical elastic tensor with both major and minor symmetry exhibits 21 constants instead.

When the lattice is subjected to a uniform external loading, it deforms uniformly as well due to the periodic microstructure, which can be represented by the singum of Node 0 in Fig. 1(b). During the deformation, the bond changes with the coordinates. For example, the bond between Nodes 0 and 1 can be represented by a vector $\mathbf{r} = \mathbf{x}^1 - \mathbf{x}^0$ with the length $r = |\mathbf{x}^1 - \mathbf{x}^0|$. Here $\mathbf{x}^0$ represents the singum node and $\mathbf{x}^1$ represents another node bonded to the singum. The singum model is built on the following assumptions [41]:

1. The interaction between nodes is governed by the bond's potential function $V(r)$.

2. The interaction between two neighboring singums is through the surface stress vector along their interface edge, and is equivalent to the bond force between the two nodes.

3. All forces on the boundary or the center of WS cell of the lattice, which are seen on the nodes and bond cutting points, will be conserved on the singum with a homogeneous elastic tensor.

For simplicity, this paper assumes the regular hexagonal lattice keeps the same shape. Otherwise, more general formulation for the hexagon with different lengths and angles shall be applied. This simplification makes the lattice to be under the hydrostatic deformation only to maintain the regular hexagonal shape. In addition, this paper assumes all bonds share the same linear elastic coefficient, so that we can use a single potential function for all bonds, although the model can be extended to different bonds that require the different

potential functions accordingly and to the bonds with nonlinear force-displacement relationship.

The force of a bond changing with its length $r = 2l_p$ can be written as

$$f_i = \frac{dV}{dr} n_i = V_{,r} n_i = \frac{1}{2l_p^0} V_{,\lambda} n_i, \tag{4}$$

where $\mathbf{n} = \frac{\mathbf{x}-\mathbf{x}^0}{|\mathbf{x}-\mathbf{x}^0|}$, λ is the stretch ratio of the center-center distance, or bond length, $\lambda = \frac{r}{2l_p^0} = \frac{l_p}{l_p^0}$. For simplicity, $\mathbf{x}^0 = \mathbf{0}$ by setting the origin at the singum node. Here the tensile force in the bond is taken as positive along $\mathbf{n}$ to be consistent with the sign convention of stresses. The potential function can be written as

$$V(r) = \frac{k}{2}(r - 2l_p^0)^2; \quad V(\lambda) = 2k(l_p^0)^2(\lambda - 1)^2, \tag{5}$$

where k can be the spring coefficient if the bond is a spring. For an elastic bond with a Young's modulus E, initial length l_p^0 with zero force, and cross-sectional area A at the stress-free state, we can write $k = \frac{EA}{2l_p^0}$.

Therefore, the forces in a physical lattice is simplified into a force network along the links or bonds. The effective stiffness can be characterized by the displacement variation caused by a small external force on the boundary. Although the local stress in the physical lattice cannot be evaluated, the effective elastic tensor can be evaluated by the average stress and strain over the singum. Two Lemmas in the previous paper [41] are restated as follows with minor revisions to define the average stress and strain over the singum, called singum stress and singum strain:

Lemma 1 *When a singum contains a node with a force $\boldsymbol{b}^S(\boldsymbol{x}^S)$ and N bond cutting points on the boundary with bonding forces $\boldsymbol{f}^I(\boldsymbol{x}^I)$ $(I = 1, 2, \ldots, N)$, which are in equilibrium with $b_i^S + \sum_{I=1}^N f_i^I = 0$, the average Cauchy stress over the singum, called singum stress, can be written as $s_{ij} = \frac{x_i^S b_j^S + \sum_{I=1}^N x_i^I f_j^I}{V_s}$.*

Proof Consider the equivalent continuum particle of the singum with the point forces on the boundary and the central node. The boundary value problem can be set up with the equilibrium equation as

$$\sigma_{ij,i} + b_j^S \delta(\mathbf{x} - \mathbf{x}^S) = 0, \tag{6}$$

where $\delta(\mathbf{x})$ is a Dirac Delta function. The boundary condition is written as

$$\sigma_{ij} n_i = \sum_{I=1}^{N} f_j^I \delta(\mathbf{x}\text{-}\mathbf{x}^I) \quad \text{for } \mathbf{x} \in \partial V_S, \tag{7}$$

where V_S denotes the volume of the singum. The stress integral can be obtained by

$$S_{ij} = \int_{V_S} \sigma_{ij}(\mathbf{x}) d\mathbf{x} = \int_{\partial(V_S)} n_k \sigma_{kj} x_i d\mathbf{x} - \int_{V_S} \sigma_{kj,k} x_i d\mathbf{x} = x_i^S b_j^S + \sum_{I=1}^{N} x_i^I f_j^I, \tag{8}$$

so that the singum stress is defined as the average Cauchy stress over the singum:

$$s_{ij} = \frac{S_{ij}}{V_s} = \frac{x_i^S b_j^S + \sum_{I=1}^{N} x_i^I f_j^I}{V_s}. \tag{9}$$

□

For central symmetric lattices under a static load, $\mathbf{b}^S$ shall always be zero, so that the singum stress in Fig. 1(b) is simplified into:

$$s_{ij} = \frac{\sum_{I=1}^{6} x_i^I f_j^I}{V_s}, \tag{10}$$

where $V_S = 2\sqrt{3}l_p^2$ is the area for the hexagonal singum. Note that the index order i and j is not sensitive when the stress is symmetric, which has not been differentiated in the previous paper [40] yet. However, this paper normalizes the order for the asymmetry of stress in general cases.

Lemma 2 *When a 2D singum contains N bond cutting points on the center-point of each side of the boundary with outward normal direction* $\boldsymbol{n}^I$, *length* L^I, *and displacement* $\boldsymbol{u}^I$ *in corresponding to the* I*th cutting point, the average displacement gradient over the singum, called singum strain, can be written as* $d_{ij} = \frac{\sum_{I=1}^{N} L^I u_i^I n_j^I}{V_s}$. *Similarly, it can be generalized to 3D singums with boundary surfaces by replacing lengths with surface areas.*

Proof The average of the DG integral over the singum, i.e. singum strain, can be written as

$$d_{ij} = \frac{\int_{V_S} u_{j,i} d\mathbf{x}}{V_s} = \frac{\int_{\partial V_S} n_i u_j d\mathbf{x}}{V_s} = \frac{\sum_{I=1}^{N} L^I n_i^I u_j^I}{V_s}. \tag{11}$$

Because all points on the same line or plane surface share the same $\mathbf{n}^I$ and the displacement in the straight line or flat plane is linear, the displacement integral can be represented by the central point, we can use the displacement at the bond cutting point to derive the surface integral. □

The average DG of the singum, called the singum strain, in Fig. 1(b) is written as follows:

$$d_{ij} = \frac{2l_p}{\sqrt{3}V_s} \sum_{I=1}^{6} n_i^I u_j^I = \frac{1}{3l_p} \sum_{I=1}^{6} n_i^I u_j^I, \tag{12}$$

which is not symmetric as the conventional strain tensor.

Therefore, the singum of Node 0 is constructed with the singum stress and strain defined by the force and displacement of the cutting points on the singum surface. Note that the volume integrals of stress and strain in a continuum domain is transferred to its boundary [39]. Due to the straight edge of singum particle and Dirac Delta function as the point forces at the cutting points, the stress and strain are exactly obtained for the lattices with hinge connections, which creates a way to derive the stiffness of the lattices exactly.

2.2 The Stiffness of the Singum of a Hexagonal Lattice

The stiffness of the singum can be tested by applying an incremental DG variation δd_{ij} at every point $\mathbf{x}$. Following the Cauchy–Born rule [34], an affine transformation of the lattice will be induced with the displacement variation as follows:

$$\delta u_j = x_i \delta d_{ij}, \tag{13}$$

which will induce the bond length variation and volume variation, and thus the singum stress variation from Eq. (10) as

$$\delta s_{ij} = \frac{\sum_{I=1}^{6} \left(x_i^I f_{j,l}^I \delta x_l + \delta x_i f_j^I - x_i^I f_j^I \frac{\delta V_s}{V_s} \right)}{V_s}, \tag{14}$$

which includes three parts: the first contributed by the force variation, the second by the cutting point variation, and the third by the volume change. The last two parts are related to the configuration variation of the singum, and are called the configurational stress variation.

Considering $\delta x_k = \delta u_k$, $\delta V_s = \delta d_{ii} V_s$, $r = 2|\mathbf{x}^I| = 2l_p$, $n_i^I = x_i^I / l_p$ in the local spatial coordinate with the origin at Node 0, and $f_{j,l} = 2V_{,rr} n_j n_l + V_{,r} n_{j,l}$ along with Eqs. (4) and (13), one can rewrite Eq. (14):

$$\delta s_{ij} = \frac{1}{V_s} \sum_{I=1}^{6} \left[x_i^I x_k^I \delta d_{kl} \left(\frac{V_{,\lambda\lambda} n_j^I n_l^I}{2(l_p^0)^2} + \frac{V_{,\lambda} n_{j,l}^I}{2l_p^0} \right) + x_k^I \delta d_{ki} \frac{V_{,\lambda} n_j^I}{2l_p^0} - x_i^I \frac{V_{,\lambda} n_j^I}{2l_p^0} \delta d_{kk} \right]. \tag{15}$$

Using $x_i^I = n_i^I \lambda l_p^0$ and $n_{j,l} = \frac{\delta_{jl} - n_j n_l}{l_p}$, one can reorganize the above equation into

$$\delta s_{ij} = \frac{1}{2V_s} \sum_{I=1}^{6} \left[(\lambda^2 V_{,\lambda\lambda} - \lambda V_{,\lambda}) n_i^I n_j^I n_k^I n_l^I + \lambda V_{,\lambda} (\delta_{jl} n_i^I n_k^I + \delta_{il} n_j^I n_k^I - \delta_{kl} n_i^I n_j^I) \right], \delta d_{kl} \tag{16}$$

which can be simplified as

$$\delta s_{ij} = C_{ijkl} \delta d_{kl}, \tag{17}$$

where C_{ijkl} indicates the stiffness of singum related the variations of the singum stress and strain as

$$C_{ijkl} = \frac{1}{2V_s} \sum_{I=1}^{6} (\lambda^2 V_{,\lambda\lambda} - \lambda V_{,\lambda}) n_i^I n_j^I n_k^I n_l^I + \lambda V_{,\lambda} (\delta_{jl} n_i^I n_k^I + \delta_{il} n_j^I n_k^I - \delta_{kl} n_i^I n_j^I) \tag{18}$$

where the superscript I of V^I can be disregarded because each pair of the bond share the same center-center distance $2l_p$. The summation in Eq. (18) is reduced to the summation of $n_i^I n_j^I$ and $n_i^I n_j^I n_k^I n_l^I$, which can be written in the following identities for the hexagonal lattice:

$$\sum_{I=1}^{6} n_i^I n_j^I = 3\delta_{ij}; \quad \sum_{I=1}^{6} n_i^I n_j^I n_k^I n_l^I = \frac{3}{4} (\delta_{ij}\delta_{kl} + \delta_{ik}\delta_{jl} + \delta_{il}\delta_{jk}). \tag{19}$$

Substituting Eq. (19) into Eq. (18) with $V_s = 2\sqrt{3}l_p^2 = 2\sqrt{3}\lambda^2(l_p^0)^2$, the relation between the stiffness tensor $\mathbf{C}$ of hexagonal lattice and the potential can be written as

$$C_{ijkl} = \frac{\sqrt{3}}{16\lambda(l_p^0)^2}\left[(\lambda V_{,\lambda\lambda} - 5V_{,\lambda})\delta_{ij}\delta_{kl} + (\lambda V_{,\lambda\lambda} + 3V_{,\lambda})(\delta_{ik}\delta_{jl} + \delta_{il}\delta_{jk})\right] \tag{20}$$

where the potential $V(\lambda)$ is defined in Eq. (5). However, the above equation is applicable to general potentials, such as interatomic potential for crystal lattices [9, 42] and Hertz's contact based potential for granular lattices [45]. For example, in our recent work for the packed cylinder lattices [45], the formulation was developed with Hertz's contact based potential and verified by the numerical simulation of a large assembly of cylinders. The numerical results rapidly converge to the singum model prediction, which confirms the exactness of Eq. (20).

It is interesting that the hexagonal lattice exhibits an isotropic elastic tensor in the 2D space, although it exhibits an angular shape of the unit cell or singum. Although DG is not symmetric, the stress induced on the singum is always symmetric, and both d_{12} and d_{21} produce the same stress tensor. Therefore, the singum stress-strain relationship can recover the classical stress-strain relationship [45]. When the lattice exhibits zero prestress, the Poisson's ratio under a uniaxial loading in 2D is 1/3 [45].

Note that most other central symmetric lattices exhibit anisotropic elastic behavior with a certain orientation stiffer than others [45]. Particularly, in 3D cases, no lattice is found to provide an isotropic elasticity tensor yet unless an orientational average is applied for polycrystal lattices [40, 43].

3 Singum Model of a Honeycomb Lattice Without Central Symmetry

Figure 2(a) shows a honeycomb lattice in which each node connects with 3 nodes forming hexagons, and no central symmetry exists. A single singum particle cannot fill the space seamlessly with the periodic translation of the singum. A primitive cell shall include two singums. For example. the singums of nodes A and B in Fig. 2(b) can seamlessly fill the 2D space without any rotation, and thus their combination can form primitive cell AB. Notice the lattice with hinged joints in Fig. 2(a) is not statically determinate. However, given a displacement controlled load with Eq. (13), the lattice still exhibits stiffness as long as the DG is not overlapped with the free-rigid motion mode of the bonds. Particularly, when prestress exists in the lattice, the stiffness changes significantly as well.

3.1 Singum Construction and Equilibrium

The similar procedure of the regular hexagonal lattices can be applied to the honeycomb lattice as well, but the equilibrium of the singum will be questionable. Note that in the earlier paper [40], the honeycomb lattice was mentioned as a hexagonal atomic lattice for graphene. In this paper, because both lattices are mentioned, we use the term of "honeycomb lattice" to differentiate it from a regular hexagonal lattice.

Using the Cauchy–Born rule, given a DG variation δd_{ij}, the displacement variation will lead to a force variation of each bond, which leads to a resultant force on each singum. Here the resultant force caused by the three bonds on singum B can be written as [41]:

$$\delta P_i^B = \sum_{I=1}^{3} \delta f_i^I \text{ with } \delta f_i^I = \frac{1}{2l_p^0}\left[(\lambda V_{,\lambda\lambda} - V_{,\lambda})n_i^I n_k^I n_l^I + V_{,\lambda} n_k^I \delta_{il}\right]\delta d_{kl}. \tag{21}$$

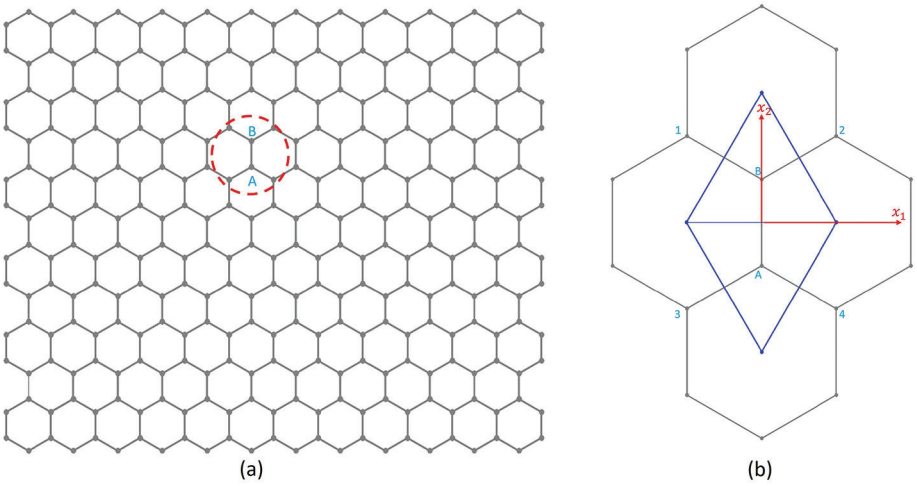

Fig. 2 The singum modeling of a honeycomb lattice: (a) the overall honeycomb lattice with two nodes highlighted and (b) primitive cell AB containing the singum particles of Nodes A and B

Because the bonds in singum A are in mirror reflection of those in singum B, one can obtain $\delta P_i^A = -\delta P_i^B$, which will distort the lattice within the primitive cell with more than one singums. However the periodic boundary condition at the four cutting points on the primitive cell AB shall still follow the displacement in Eq. (13), so that the given displacement gradient can be achieved over the primitive cell.

These forces will cause the nodes A and B to move with central symmetry referring to the mid-point of AB and the forces will be redistributed among the bonds for equilibrium. Generalizing *Lemma 2* to a primitive cell with two singums A and B, as long as the displacement variations of the four bond-cutting points satisfy the periodic boundary condition corresponding to a uniform strain $\delta\mathbf{d}$, no matter how nodes A and B move inside the primitive cell, the average strain variation on the primitive cell will remain the same as $\delta\mathbf{d}$.

To calculate the effective stress over primitive cell AB, we cite two Lemmas [41] as follows:

Lemma 3 *When a singum is in equilibrium under a set of forces on the node and bond cutting points, the average stress of the singum is independent of the translation of the Cartesian coordinate.*

Therefore, the effective stress and DG of a singum in an equilibrium stress state are independent of the selection of the coordinates, so that the local coordinate with the origin on the node can be used for convenience of derivation.

Lemma 4 *When two contacting singums with* $\boldsymbol{b}^1(\boldsymbol{X}^1) = -\boldsymbol{b}^2(\boldsymbol{X}^2)$ *on their central nodes, each of which is in equilibrium, merge into a large cell, the stress integral over the large cell is equal to the sum of the stress integrals over the two singums and* $\boldsymbol{b}^1(\boldsymbol{X}^1 - \boldsymbol{X}^2)$.

When primitive cell AB is subjected to a displacement variation at the four cutting point in accordance with $\delta\mathbf{d}$ by Eq. (13), the prestress and force variation on nodes A and B shall

reach equilibrium. Following Eq. (14), the Cauchy stress variation from Eq. (10) is written as

$$\delta s_{ij} = \frac{\sum_{I=1}^{4} \left(x_i^I \delta f_j^I + x_k \delta d_{ki} f_i^I - x_i^I f_j^I \delta d_{kk} \right)}{2V_s}, \tag{22}$$

where the last two parts of configurational stress are given by the displacement gradient variation and pre-stress with $\mathbf{f}^I$ given in Eq. (4), which satisfies the equilibrium condition as the four cutting points exhibit two pairs of $\mathbf{n}$ in opposite directions and is independent of the coordinate selection; and the first part will be different from the last section because the Cauchy–Born rule leads to the loss of the equilibrium of nodes A and B. However, it can be decomposed into two cases, both of which satisfy the equilibrium condition:

Case I: *A uniform displacement field in the whole unit cell following the Cauchy–Born rule [34], which will generate the force variations on each bond following Eq. (4).*

In this case, the DG satisfies the displacement load, but the force cannot reach equilibrium with resultant forces of ($\delta\mathbf{P}^B$ and $\delta\mathbf{P}^A$) on the nodes B and A, respectively. To physically achieve this deformation statically, inverse forces of ($-\delta\mathbf{P}^B$ and $-\delta\mathbf{P}^A$) are required on A and B, respectively.

Case II: *The 4 bond cutting points of the unit cell are fixed, and the two forces* ($\delta\mathbf{P}^B$ *and* $\delta\mathbf{P}^A$) *are applied on B and A, respectively, which yields reactions on the four cutting points and the force on AB.*

This loading case will not generate any effective DG in the lattice because the four points are fixed with zero displacement; whereas effective stresses are generated with the reactions at the cutting points and the forces on nodes A and B. Note that the primitive cell AB satisfied both central symmetry to the mid-point of AB and the mirror symmetry to the perpendicular mid-line of AB. Due to the mirror symmetry and Eq. (21), $\delta P_i^A = -\delta P_i^B$; due to the central symmetry, the mid-point of AB will be fixed as well. Therefore, the deformed primitive cell AB will also satisfy the central symmetry in Case II. Consequently, one can focus on one singum with three cutting points fixed, which can represent the other through the central symmetry.

Use singum B as an example. Given a force $f_i = 1$ $(i = 1, 2)$ on note B with the coordinate origin set up at B as well, it will be transferred to three cutting points as R_{ij}^I, where $I = 1, 2, 3$ represents the cutting points of the Ith bar and $j = 1, 2$ indicates the force components in x_1 and x_2 caused by a unit force f_i. Notice that due to the configuration changes, the force variation in each bar will not be on the same orientation as the bar. A structural analysis of this three-bond indeterminate structure with a three-hinge support will provide R_{ij}^I. For singum B, it is obtained as:

$$\begin{aligned} R_{ij}^1 &= \begin{pmatrix} -\frac{2(\lambda-1)}{3(2\lambda-1)} & 0 \\ 0 & -\frac{2\lambda}{3(2\lambda-1)}) \end{pmatrix}; R_{ij}^2 = \begin{pmatrix} -\frac{4\lambda-1}{6(2\lambda-1)} & \frac{\sqrt{3}}{6(2\lambda-1)} \\ \frac{\sqrt{3}}{6(2\lambda-1)} & -\frac{4\lambda-3}{6(2\lambda-1)} \end{pmatrix}; \\ R_{ij}^3 &= \begin{pmatrix} -\frac{4\lambda-1}{6(2\lambda-1)} & -\frac{\sqrt{3}}{6(2\lambda-1)} \\ -\frac{\sqrt{3}}{6(2\lambda-1)} & -\frac{4\lambda-3}{6(2\lambda-1)} \end{pmatrix}. \end{aligned} \tag{23}$$

The detail steps to derive the force transfer matrix $\mathbf{R}$ are elaborated in Appendix A. Given the force variation δP_i^B, the force variation on the three bonds are given as

$$\delta T_j^I = \delta P_m^B R_{mj}^I. \tag{24}$$

For different lattices without central symmetry, the force transfer matrix can be determined in the same fashion.

3.2 The Stiffness of the Singum of a Honeycomb Lattice

The superposition of the two cases makes both the periodic boundary condition of the unit cell and the equilibrium condition of the nodes satisfied, and thus forms the solution to the original problem. Now both cases satisfy the equilibrium with forces on nodes A and B, and thus *Lemmas 3* and *4* can be applied, so that the local coordinate of each singum with three bonds can be used to represent the overall primitive cell AB. The average stress in primitive cell AB can be the mean value of the average stress of singum A and singum B.

The superposition of Case I and II for the singum B can be written as:

$$\delta s_{ij} = \sum_{I=1}^{3} \left[\frac{x_i^I (\delta f_j^I + \delta T_j^I)}{V_s} + \frac{x_k^I \delta d_{ki} f_j^I}{V_s} - \frac{x_i^I f_j^I \delta d_{kk}}{V_s} \right], \tag{25}$$

where the forces on Node B in two cases are eliminated by each other, and the configuration stress variation in Case II is zero due to the fixed cutting points. Substituting $\delta \mathbf{f}^I$ and $\delta \mathbf{T}^I$ in Eqs. (21) and (24) into the above equation, similarly to Eq. (16), one can obtain:

$$\begin{aligned} \delta s_{ij}^B = & \frac{1}{2V_s} \sum_{I=1}^{3} \left[(\lambda^2 V_{,\lambda\lambda} - \lambda V_{,\lambda}) n_i^I n_j^I n_k^I n_l^I + \lambda V_{,\lambda} (\delta_{jl} n_i^I n_k^I + \delta_{il} n_j^I n_k^I - \delta_{kl} n_i^I n_j^I) \right] \delta d_{kl} \\ & + \frac{1}{2V_s} \sum_{I=1}^{3} \sum_{J=1}^{3} \left[(\lambda^2 V_{,\lambda\lambda} - \lambda V_{,\lambda}) R_{mj}^I n_m^J n_i^I n_k^J n_l^J + \lambda V_{,\lambda} R_{lj}^I n_i^I n_k^J \right] \delta d_{kl}. \end{aligned} \tag{26}$$

Similarly, one can obtain δs_{ij}^A. Considering the mirror symmetry between singums A and B of $\mathbf{n}^I$ and $\mathbf{R}^I$, one can see that δs_{ij}^A shares the same average stress, so that the effective stiffness tensor can be obtained as:

$$C_{ijkl} = \frac{1}{2V_s} \left[\lambda V_{,\lambda} E_{ijkl}^1 + (\lambda^2 V_{,\lambda\lambda} - \lambda V_{,\lambda}) E_{ijkl}^2 \right]. \tag{27}$$

where the tensors $\mathbf{E}^1$ and $\mathbf{E}^2$ are written as

$$\begin{aligned} E_{ijkl}^1 &= \sum_{I=1}^{3} (\delta_{jl} n_i^I n_k^I + \delta_{il} n_j^I n_k^I - \delta_{kl} n_i^I n_j^I) + \sum_{I=1}^{3} \sum_{J=1}^{3} R_{lj}^I n_i^I n_k^J, \\ E_{ijkl}^2 &= \sum_{I=1}^{3} n_i^I n_j^I n_k^I n_l^I + \sum_{I=1}^{3} \sum_{J=1}^{3} R_{mj}^I n_m^J n_i^I n_k^J n_l^J. \end{aligned} \tag{28}$$

To demonstrate the general fourth-rank tensor $\mathbf{E}$, we generalize the Voigt notation as $11 \to 1$, $22 \to 2$, $12 \to 3$, and $21 \to 4$, so that $\mathbf{E}$ is transformed into a 4×4 matrix of $\mathbf{E}$ as follows:

$$\mathbf{E} = \begin{pmatrix} E_{1111} & E_{1122} & E_{1112} & E_{1121} \\ E_{2211} & E_{2222} & E_{2212} & E_{2221} \\ E_{1211} & E_{1222} & E_{1212} & E_{1221} \\ E_{2111} & E_{2122} & E_{2112} & E_{2121} \end{pmatrix}. \tag{29}$$

Similarly to Eq. (19), one can obtain

$$\sum_{I=1}^{3} n_i^I n_j^I = \frac{3}{2} \delta_{ij}; \quad \sum_{I=1}^{3} n_i^I n_j^I n_k^I n_l^I = \frac{3}{8} (\delta_{ij}\delta_{kl} + \delta_{ik}\delta_{jl} + \delta_{il}\delta_{jk}), \tag{30}$$

which are independent from the coordinate, but can be easily checked by defining $\mathbf{n}^1 = (0, -1)$, $\mathbf{n}^2 = (-\frac{\sqrt{3}}{2}, \frac{1}{2})$, and $\mathbf{n}^3 = (\frac{\sqrt{3}}{2}, \frac{1}{2})$ in Fig. 2(b).

Using Eqs. (30) and (23) in Eq. (28) with the above definition of $\mathbf{n}^I$, one can obtain the matrix form of $\mathbf{E}^1$ and $\mathbf{E}^2$ as:

$$\mathbf{E}^1 = \begin{pmatrix} \frac{3}{2} & -\frac{3}{2} & 0 & 0 \\ -\frac{3}{2} & \frac{3}{2} & 0 & 0 \\ 0 & 0 & \frac{3}{2} & \frac{3}{2} \\ 0 & 0 & \frac{3}{2} & \frac{3}{2} \end{pmatrix}; \quad \mathbf{E}^2 = \begin{pmatrix} \frac{3(3\lambda-2)}{4(2\lambda-1)} & \frac{3\lambda}{4(2\lambda-1)} & 0 & 0 \\ \frac{3\lambda}{4(2\lambda-1)} & \frac{3(3\lambda-2)}{4(2\lambda-1)} & 0 & 0 \\ 0 & 0 & \frac{3(\lambda-1)}{4(2\lambda-1)} & \frac{3(\lambda-1)}{4(2\lambda-1)} \\ 0 & 0 & \frac{3(\lambda-1)}{4(2\lambda-1)} & \frac{3(\lambda-1)}{4(2\lambda-1)} \end{pmatrix}. \tag{31}$$

Actually, both $\mathbf{E}^1$ and $\mathbf{E}^2$ for a honeycomb lattice is isotropic, and can be written as

$$\begin{aligned} E^1_{ijkl} &= -\frac{3}{2}\delta_{ij}\delta_{kl} + \frac{3}{2}(\delta_{ik}\delta_{jl} + \delta_{il}\delta_{jk}); \\ E^2_{ijkl} &= \frac{3\lambda}{4(2\lambda-1)}\delta_{ij}\delta_{kl} + \frac{3(\lambda-1)}{4(2\lambda-1)}(\delta_{ik}\delta_{jl} + \delta_{il}\delta_{jk}). \end{aligned} \tag{32}$$

which yields the effective stiffness tensor of a honeycomb lattice at $\lambda = 1$ as

$$C_{ijkl}|_{\lambda=1} = \frac{\sqrt{3}}{24(l_p^0)^2} V_{,\lambda\lambda}\delta_{ij}\delta_{kl}, \tag{33}$$

where $V_s = 3\sqrt{3}l_p^2 = 3\sqrt{3}\lambda^2(l_p^0)^2$ and $V_{,\lambda} = 0$ are used. It is significantly different from Eq. (20) because the equilibrium of the singum particle releases energy from the state with the Cauchy–Born rule by the superposition of the second case. When the bonds are in the unstressed state of $\lambda = 1$, the Poisson's ratio $\nu = 1$, the shear modulus $\mu = 0$ and the lattice is not stable. However, when it is prestressed, the shear modulus can be non-zero. The isotropic elastic behavior and symmetry may be lost. Here the isotropic symmetry only exists for an equilateral triangular singum with the singum node at the centroid. Otherwise, when $\sum_{J=1}^{3} n_l^J$ is not zero, the effective stiffness will not only become anisotropic, but also lose the minor symmetry due to the last term $\mathbf{E}^1$ in Eq. (28), which will be demonstrated in the next Section of auxetic lattices. The generalized Voigt notation in Eq. (29) can be applicable to those cases. Note that the honeycomb lattice has been widely studied for graphene's atomic lattice structure as well with different types of interatomic potentials [18, 40]. Besides the 2D analysis, the out-of-plane deformation has been studied as well [7, 31].

To illustrate the calculation of the above formulation, a numerical case study is conducted with a honeycomb truss system in Appendix B. Note that this paper address the lattice with harmonic potential or spring bonds of neighboring nodes, which is different from the stanine or graphene lattices with long-range atomic interactions in the literature [8, 32]. For instance, in Fig. 2(b), node B only interacts with nodes 1, 2, and A through the spring bonds; whereas in atomic lattices of graphene or stanine, node B also interacts with nodes 3, 4, and all others, whose force intensity decays with the distance in the corresponding potential function. As a result, the honeycomb truss system is structurally unstable without prestress, but exhibits stiffness in a certain deformation mode, which the singum model can demonstrate very well. When prestress exists, for example, in Appendix B, the stiffness tensor in the generalized

Voigt notation is written as

$$\mathbf{C} = \frac{\sqrt{3}K}{6\lambda(2\lambda-1)} \begin{pmatrix} \lambda(4\lambda-3) & -(4\lambda^2-7\lambda+2) & 0 & 0 \\ -(4\lambda^2-7\lambda+2) & \lambda(4\lambda-3) & 0 & 0 \\ 0 & 0 & 4\lambda^2-5\lambda+1 & 4\lambda^2-5\lambda+1 \\ 0 & 0 & 4\lambda^2-5\lambda+1 & 4\lambda^2-5\lambda+1 \end{pmatrix}. \tag{34}$$

If $\lambda = 1.1$, then the stiffness tensor becomes:

$$\mathbf{C} = \begin{pmatrix} 0.3368k & 0.1881k & 0 & 0 \\ 0.1881k & 0.3368k & 0 & 0 \\ 0 & 0 & 0.0744k & 0.0744k \\ 0 & 0 & 0.0744k & 0.0744k \end{pmatrix}, \tag{35}$$

which shows that the shear modulus is indeed not zero anymore. If $\lambda < 1$, the lattice is not stable at all, as the shear modulus exhibits a negative value.

4 Singum Model of an Auxetic Lattice

In the last two sections, the lattices may commonly be found in nature. When those lattices are subjected to hydrostatic loading, the lattice deformation is isotropic with the same $\mathbf{n}^I$ and the effective stiffness can be predicted with λ changing. However, when the lattices are subjected to an arbitrary load, the microstructure of the lattice may distort and become another type of lattice, and the vectors $\mathbf{n}^I$ may not satisfy the identities in Eqs. (19) and (30) and the effective material will become anisotropic. In addition, one can also purposely fabricate a lattice in Fig. 3(a), whose singum shape in Fig. 3 (b) becomes an isosceles trapezoid and Node B is not at the centroid of singum B anymore. The lattice is an example of an auxetic lattice which exhibits a negative Poisson's ratio.

4.1 Singum Construction and Modeling

Similarly to the honeycomb lattice, this auxetic is not stable and a single singum particle cannot represent the lattice periodically. However, a primitive cell AB can represent it. Assume all links share the same length, the microstructure can be represented by α in Fig. 3(b). Specifically, when $\alpha = 2\pi/3$, the lattice recovers the honeycomb lattice, and the singum is an equilateral triangle. When $\pi/2 \le \alpha < 2\pi/3$, the singum at B becomes an upward isosceles trapezoid [41]. When $\pi/3 \le \alpha < \pi/2$, the singum at B becomes a downward isosceles trapezoid in Fig. 3(b). With the decrease of α from $2\pi/3$ toward $\pi/3$, the bond length I_p does not change, but the area changes with α as follows:

$$V_s = 4l_p^2 \sin^2\alpha \tan\frac{\alpha}{2}, \tag{36}$$

where the height of the trapezoid $2l_p(1-\cos\alpha)$, the bottom edge length $2l_p \tan\frac{\alpha}{2}$, and the top edge length $2l_p(1+2\cos\alpha)\tan\frac{\alpha}{2}$ are used. Therefore, the density increase three times or the area decrease to one third from $3\sqrt{3}l_p^2$ to $\sqrt{3}l_p^2$ for $\alpha = 2\pi/3$ and $\pi/3$, respectively.

Using the geometry in Fig. 3(b) at $\alpha = \pi/3$, one can obtain the directional norms of singum B as $\mathbf{n}^1 = (0,-1)$, $\mathbf{n}^2 = (\frac{\sqrt{3}}{2}, -\frac{1}{2})$, and $\mathbf{n}^3 = (-\frac{\sqrt{3}}{2}, -\frac{1}{2})$. The singum node $(0,0)$ is

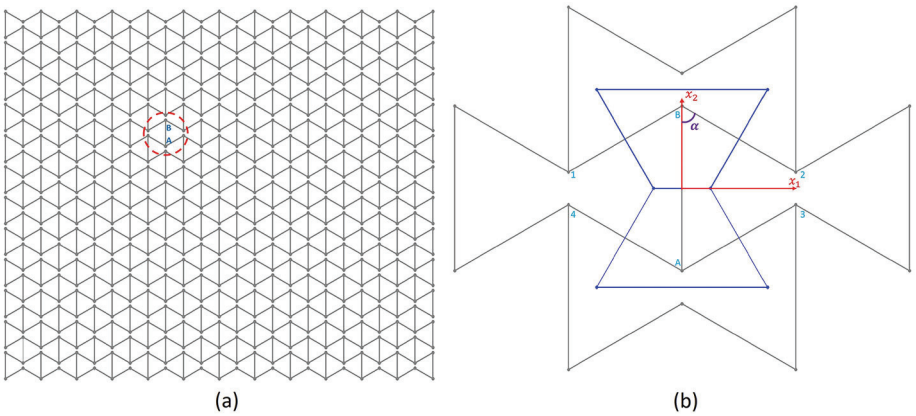

Fig. 3 The singum modeling of an auxetic lattice: (a) the overall auxetic lattice with two nodes highlighted and (b) primitive cell AB containing the singum particles of Nodes A and B

not at the centroid of the singum particle anymore but the midpoint of the top edge. When it is stretched in the horizontal or vertical direction, the lattice is expanded in the perpendicular direction as well, which makes an auxetic material with a negative Poisson's ratio.

Following the same procedure as the last section, one can derive the stiffness. However, because $\sum_{J=1}^{3} n_2^J = -2$, the stiffness matrix will be much more complex. When a stretch ratio $\lambda \neq 1$ is applied to the lattice, to maintain the shape of the auxetic lattice, dipole forces are required on each pair of singums in a primitive cell. Otherwise, the lattice cannot reach the equilibrium state. Given an arbitrary λ for the lattice in Fig. 3, one can calculate the required dipole forces on A and B. On B, the required force is

$$\mathbf{D}^B = -\sum_{I=1}^{3} \frac{1}{2l_p^0} V_{,\lambda} \mathbf{n}^I = 2kl_p^0(\lambda - 1)\begin{pmatrix} 0 \\ 2 \end{pmatrix}. \tag{37}$$

Keeping the force constant, the lattice will exhibit a certain loading resistance shown by the stiffness tensor as well.

Following Appendix A, one can introduce a DG variation, which leads to the change of the microstructure. The redistribution matrix of R_{ij}^I can be obtained by the static analysis with a unit force on x_1 or x_2, respectively, which is written as

$$\begin{aligned} R_{ij}^1 &= \begin{pmatrix} -\frac{2(\lambda-1)}{3(2\lambda-1)} & 0 \\ 0 & -\frac{2\lambda}{3(2\lambda-1)}) \end{pmatrix}; R_{ij}^2 = \begin{pmatrix} -\frac{4\lambda-1}{6(2\lambda-1)} & \frac{\sqrt{3}}{6(2\lambda-1)} \\ \frac{\sqrt{3}}{6(2\lambda-1)} & -\frac{4\lambda-3}{6(2\lambda-1)} \end{pmatrix}; \\ R_{ij}^3 &= \begin{pmatrix} -\frac{4\lambda-1}{6(2\lambda-1)} & -\frac{\sqrt{3}}{6(2\lambda-1)} \\ -\frac{\sqrt{3}}{6(2\lambda-1)} & -\frac{4\lambda-3}{6(2\lambda-1)} \end{pmatrix}. \end{aligned} \tag{38}$$

The force transfer in the lattice is significantly different from the regular hexagonal lattice, which causes anisotropic stiffness. As shown subsequently, $u_{1,2}$ and $u_{2,1}$ will produce different stress states, so the traditional Voigt notation will not be sufficient to describe the constitutive law.

Using the general asymmetric notation in Eq. (29), one can obtain:

$$E^1_{IJ} = \begin{pmatrix} \frac{3}{2} & -\frac{6\lambda-1}{2(2\lambda-1)} & 0 & 0 \\ -\frac{3}{2} & \frac{2\lambda-3}{6(2\lambda-1)} & 0 & 0 \\ 0 & 0 & \frac{3}{2} & \frac{6\lambda-5}{2(2\lambda-1)} \\ 0 & 0 & \frac{3}{2} & \frac{2\lambda+1}{6(2\lambda-1)} \end{pmatrix} \tag{39}$$

and

$$E^2_{IJ} = \begin{pmatrix} \frac{3(3\lambda-2)}{4(2\lambda-1)} & \frac{3\lambda-4}{4(2\lambda-1)} & 0 & 0 \\ -\frac{\lambda}{4(2\lambda-1)} & \frac{7\lambda-6}{12(2\lambda-1)} & 0 & 0 \\ 0 & 0 & \frac{3(\lambda-1)}{4(2\lambda-1)} & \frac{3(\lambda-1)}{4(2\lambda-1)} \\ 0 & 0 & -\frac{(\lambda-1)}{4(2\lambda-1)} & -\frac{(\lambda-1)}{4(2\lambda-1)} \end{pmatrix} \tag{40}$$

Equations (39) and (40) lose both major and minor symmetry when a prestress exists or $V_{,\lambda} \neq 0$. However, when the bond is in the unstressed state of $V_{,\lambda} = 0$, the stiffness is only related to $\mathbf{E}^2$. The lattice exhibits zero stiffness in a certain deformation mode, which is discussed below.

4.2 Negative Poisson's Ratio and Asymmetry of Stiffness

Similarly to Eq. (33), the stiffness tensor of the above lattice can be written in the generalized Voigt matrix form as:

$$\mathbf{C} = \frac{\sqrt{3}K}{6\lambda(2\lambda-1)} \begin{pmatrix} \lambda(4\lambda-3) & -\frac{\eta}{3} & 0 & 0 \\ -\frac{\eta}{3} & \frac{\lambda(4\lambda-3)}{9} & 0 & 0 \\ 0 & 0 & \beta & \frac{\gamma}{3} \\ 0 & 0 & \frac{\gamma}{3} & \frac{\beta}{9} \end{pmatrix}, \tag{41}$$

where $\eta = 12\lambda^2 - 17\lambda + 6$, $\beta = 4\lambda^2 - 5\lambda + 1$, and $\gamma = 12\lambda^2 - 19\lambda + 7$.

Consider the unstressed state of the auxetic lattice at $\alpha = \pi/3$ and $\lambda = 1$, only $\mathbf{E}^2$ contributes to the overall stiffness in Eq. (27) and all terms related to $V_{,\lambda}$ in Eq. (41) are zero. Note that the stiffness matrix in Eq. (41) exhibits a rank 1, so the lattice can deform with the rigid motion of all bonds as long as $3d_{11} = d_{22}$. Therefore, it exhibits no rigidity to shear and uniaxial loading with zero Young's modulus and shear modulus, but the Poisson's ratio is negative at -3 and $-1/3$ for uniaxial loading in x_1 and x_2 directions, respectively [41]. Given a displacement controlled test with $3d_{11} \neq d_{22}$, the lattice will exhibit stiffness through the constitutive law in Eq. (41).

Notice that the above formulation requires a pair of dipole forces in Eq. (37) in the primitive cell when $\lambda \neq 1$. Therefore, in nature without such a dipole force, an auxetic lattice in Fig. 3 cannot maintain the shape with $\alpha = \pi/3$ under a hydrostatic load, which is different from the hexagonal and honeycomb lattices. The singum model can still numerically predict the effective elasticity at any shape of the primitive cell. When a prestress is applied to the auxetic lattice, the stiffness of the lattice will be significantly different. For example, when the lattice is under a hydrostatic pressure in the 2D plane with dipole forces, the bond length proportionally reduces so that $\alpha = \pi/3$. Therefore, $V_{,\lambda} < 0$. and $\mathbf{E}^1$ will contribute to the effective stiffness of the lattice given an additional test load, which exhibits neither minor nor major symmetry. Note that the equilibrium issue of the singum will be discussed subsequently in Sect. 7.

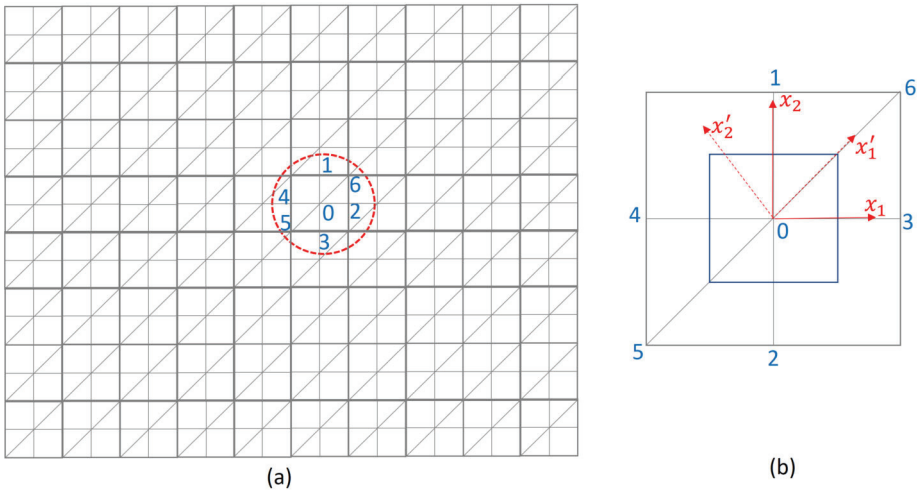

Fig. 4 The singum modeling of a square lattice with unbalanced central symmetry: (a) the overall square lattice with a representative node highlighted and (b) the singum particle of Node 0 as a primitive cell

5 Singum Model of a Square Lattice with Unbalanced Central Symmetry

In the last three cases, all bonds share the same length. This case extends to a square lattice in Fig. 4(a), which can be considered as Fig. 1 undergoing a simple shear motion in x_2 direction. Obviously, the bonds 0-2 and 0-5 exhibit a longer bond length and therefore a different potential. They strengthen the lattice in the 45° direction, so the central symmetry is not balanced. Assume all bonds are made of the same material for simplicity.

5.1 Singum Construction and Modeling

Following the same fashion, the singum of Node 0 is constructed in Fig. 4 (b), which is still a square. There are two types of bonds. Assume the unstressed bond lengths are $2l_p^0$ and $2\sqrt{2}l_p^0$ respectively. The longer bonds exhibit a lower spring coefficient of $k/\sqrt{2}$ with the new potential as

$$\overline{V}(r) = \frac{k}{2\sqrt{2}}(r - 2\sqrt{2}l_p^0)^2; \; or \quad \overline{V}(\lambda) = 2\sqrt{2}k(l_p^0)^2(\lambda - 1)^2 = \sqrt{2}V(\lambda). \tag{42}$$

The 6 directional norms are $(\pm 1, 0)$, $(0, \pm 1)$, and $\pm(1/\sqrt{2}, 1/\sqrt{2})$, and $V_s = 4l_p^2$. Because they are central symmetric, given a DG variation, following the Cauchy–Born rule, the resultant force on the singum node is always zero, so no secondary force is needed to keep it in equilibrium. Following the similar fashion in Sect. 2, one can obtain the stress variation as follows:

$$\delta s_{ij} = \frac{1}{V_s}\sum_{I=1}^{6}\left[x_i^I x_k^I \delta d_{kl}\left(\frac{V_{,\lambda\lambda}n_j^I n_l^I}{2(l_p^0)^2} + \frac{V_{,\lambda}n_{j,l}^I}{2l_p^0}\right) + x_k^I \delta d_{ki}\frac{V_{,\lambda}n_j^I}{2l_p^0} - x_i^I \frac{V_{,\lambda}n_j^I}{2l_p^0}\delta d_{kk}\right]. \tag{43}$$

Using $x_i^I = n_i^I \lambda l_p^0$ and $n_{j,l} = \frac{\delta_{jl} - n_j n_l}{l_p}$, one can reorganize the above equation into

$$\begin{aligned}\delta s_{ij} =& \frac{1}{2V_s}\sum_{I=1}^{4}\left[(\lambda^2 V_{,\lambda\lambda} - \lambda V_{,\lambda})n_i^I n_j^I n_k^I n_l^I + \lambda V_{,\lambda}(\delta_{jl} n_i^I n_k^I + \delta_{il} n_j^I n_k^I - \delta_{kl} n_i^I n_j^I)\right]\delta d_{kl} \\ &+ \frac{1}{2V_s}\sum_{I=5}^{6}\left[(\lambda^2 \overline{V}_{,\lambda\lambda} - \lambda \overline{V}_{,\lambda})n_i^I n_j^I n_k^I n_l^I \right. \\ &\left. + \lambda \overline{V}_{,\lambda}(\delta_{jl} n_i^I n_k^I + \delta_{il} n_j^I n_k^I - \delta_{kl} n_i^I n_j^I)\right]\delta d_{kl},\end{aligned} \tag{44}$$

where

$$\begin{aligned}&\sum_{I=1}^{4} n_i^I n_j^I = 2\delta_{ij}; \quad \sum_{I=1}^{4} n_i^I n_j^I n_k^I n_l^I = 2\delta_{IK}\delta_{ij}\delta_{kl}; \\ &\sum_{I=5}^{6} n_i^I n_j^I = 1; \quad \sum_{I=5}^{6} n_i^I n_j^I n_k^I n_l^I = 0.5; \\ &\overline{V}_{,\lambda\lambda} = \sqrt{2}V_{,\lambda\lambda}; \quad \overline{V}_{,\lambda} = \sqrt{2}V_{,\lambda}\end{aligned} \tag{45}$$

Therefore, one can obtain

$$\begin{aligned}C_{ijkl} =& \frac{1}{4\lambda(l_p^0)^2}\Big[(\lambda V_{,\lambda\lambda} - V_{,\lambda})(\delta_{IK}\delta_{ij}\delta_{kl} + \sqrt{2}/4) \\ &+ V_{,\lambda}[\delta_{ik}(\delta_{jl} + \sqrt{2}/2) + \delta_{jk}(\delta_{il} + \sqrt{2}/2) - \delta_{kl}(\delta_{ij} + \sqrt{2}/2))\Big].\end{aligned} \tag{46}$$

5.2 The Interpretation of the Matrix Form of the Stiffness

The stiffness tensor in Eq. (46) can be written in the generalized Voigt matrix form as:

$$\mathbf{C} = \frac{1}{4\lambda(l_p^0)^2} \times \begin{pmatrix} \frac{(4+\sqrt{2})\lambda V_{,\lambda\lambda}+\sqrt{2}V_{,\lambda}}{4} & \frac{\sqrt{2}\lambda V_{,\lambda\lambda}-(4+3\sqrt{2})V_{,\lambda}}{4} & \frac{\sqrt{2}(\lambda V_{,\lambda\lambda}+3V_{,\lambda})}{4} & \frac{\sqrt{2}(\lambda V_{,\lambda\lambda}-V_{,\lambda})}{4} \\ \frac{\sqrt{2}\lambda V_{,\lambda\lambda}-(4+3\sqrt{2})V_{,\lambda}}{4} & \frac{(4+\sqrt{2})\lambda V_{,\lambda\lambda}+\sqrt{2}V_{,\lambda}}{4} & \frac{\sqrt{2}(\lambda V_{,\lambda\lambda}-V_{,\lambda})}{4} & \frac{\sqrt{2}(\lambda V_{,\lambda\lambda}+3V_{,\lambda})}{4} \\ \frac{\sqrt{2}(\lambda V_{,\lambda\lambda}-V_{,\lambda})}{4} & \frac{\sqrt{2}(\lambda V_{,\lambda\lambda}-V_{,\lambda})}{4} & \frac{\sqrt{2}\lambda V_{,\lambda\lambda}+(4+\sqrt{2})V_{,\lambda})}{4} & \frac{\sqrt{2}\lambda V_{,\lambda\lambda}+(4+\sqrt{2})V_{,\lambda})}{4} \\ \frac{\sqrt{2}(\lambda V_{,\lambda\lambda}-V_{,\lambda})}{4} & \frac{\sqrt{2}(\lambda V_{,\lambda\lambda}-V_{,\lambda})}{4} & \frac{\sqrt{2}\lambda V_{,\lambda\lambda}+(4+\sqrt{2})V_{,\lambda})}{4} & \frac{\sqrt{2}\lambda V_{,\lambda\lambda}+(4+\sqrt{2})V_{,\lambda})}{4} \end{pmatrix} \tag{47}$$

which becomes a full matrix without zero components. This is different from the stiffness in the previous three lattices because the coordinates in the three cases are selected at the symmetric orientation, but the square lattice is not. If the coordinates rotate 45° counter-clockwise, the long bonds will be along the x_1 direction, and the stiffness tensor can be obtained by the same fashion as the above or tensor's transformation. By updating the 6

directional norms as $(\pm 1/\sqrt{2}; \pm 1/\sqrt{2})$ and $(\pm 1, 0)$, one can write

$$\begin{aligned}
&\sum_{I=1}^{4} n_i^I n_j^I = 2\delta_{ij}; \quad \sum_{I=1}^{4} n_i^I n_j^I n_k^I n_l^I = (1-2\delta_{IK})\delta_{ij}\delta_{kl} + \delta_{ik}\delta_{jl} + \delta_{il}\delta_{jk}; \\
&\sum_{I=5}^{6} n_i^I n_j^I = 2\delta_{i1}\delta_{j1}; \quad \sum_{I=5}^{6} n_i^I n_j^I n_k^I n_l^I = 2\delta_{i1}\delta_{j1}\delta_{k1}\delta_{l1}.
\end{aligned} \tag{48}$$

Therefore, the stiffness tensor becomes

$$\begin{aligned}
C'_{ijkl} = &\frac{1}{8\lambda (l_p^0)^2}\Big[(\lambda V_{,\lambda\lambda} - V_{,\lambda})[(1-2\delta_{IK})\delta_{ij}\delta_{kl} + \delta_{ik}\delta_{jl} + \delta_{il}\delta_{jk} + 2\sqrt{2}\delta_{i1}\delta_{j1}\delta_{k1}\delta_{l1}] \\
&+ V_{,\lambda}[\delta_{ik}(2\delta_{jl} + 2\sqrt{2}\delta_{j1}\delta_{l1}) + \delta_{jk}(2\delta_{il} + 2\sqrt{2}\delta_{i1}\delta_{l1}) \\
&- \delta_{kl}(2\delta_{ij} + 2\sqrt{2}\delta_{i1}\delta_{j1})]\Big]
\end{aligned} \tag{49}$$

or in the generalized Voigt matrix form as

$$\begin{aligned}
\mathbf{C}' = &\frac{1}{8\lambda (l_p^0)^2} \\
&\times \begin{pmatrix}
(1+2\sqrt{2})\lambda V_{,\lambda\lambda} + V_{,\lambda} & \lambda V_{,\lambda\lambda} - (2\sqrt{2}+3)V_{,\lambda} & 0 & 0 \\
\lambda V_{,\lambda\lambda} - 3V_{,\lambda} & \lambda V_{,\lambda\lambda} + V_{,\lambda} & 0 & 0 \\
0 & 0 & \lambda V_{,\lambda\lambda} + V_{,\lambda} & \lambda V_{,\lambda\lambda} + (1+2\sqrt{2})V_{,\lambda} \\
0 & 0 & \lambda V_{,\lambda\lambda} + V_{,\lambda} & \lambda V_{,\lambda\lambda} + (1+2\sqrt{2})V_{,\lambda}
\end{pmatrix}.
\end{aligned} \tag{50}$$

Here $C_{ijkl} = Q_{im}Q_{jn}Q_{kp}Q_{lq}C'_{mnpq}$, in which $\mathbf{Q} = \begin{pmatrix} 1/\sqrt{2} & -1/\sqrt{2} \\ 1/\sqrt{2} & 1/\sqrt{2} \end{pmatrix}$.

Given a confined uniaxial displacement load along the short bond direction, one can see both shear and normal stress will be generated from Eq. (47). However, if the confined displacement load is along the long bond direction, Eq. (50) shows that only normal stress will be generated. When no prestress exists or $V_{,\lambda} = 0$, the stiffness along the long-bond direction is much higher than the perpendicular direction.

6 Singum Model of a Chiral Lattice

The previous four types of lattices exhibit the connection between the nodes with the center-to-center bonds. A chiral lattice in Fig. (5) features internal rotational units, in the form of rigid rings connected by tangent bonds with hinge joints [33], The elastic tensor of the lattice is contributed by the bonds but changes with the ratio of the ring radius R to the center-center distance $2L$.

6.1 Singum Construction and Modeling

The singum of Node 0 is constructed in Fig. 5 (b), which is still a hexagon similar to Fig. 1(b). Note that to keep the space continuous, the WS cell is based on the center-center line instead of the bond, although the cutting point is the cross point. If the cutting line

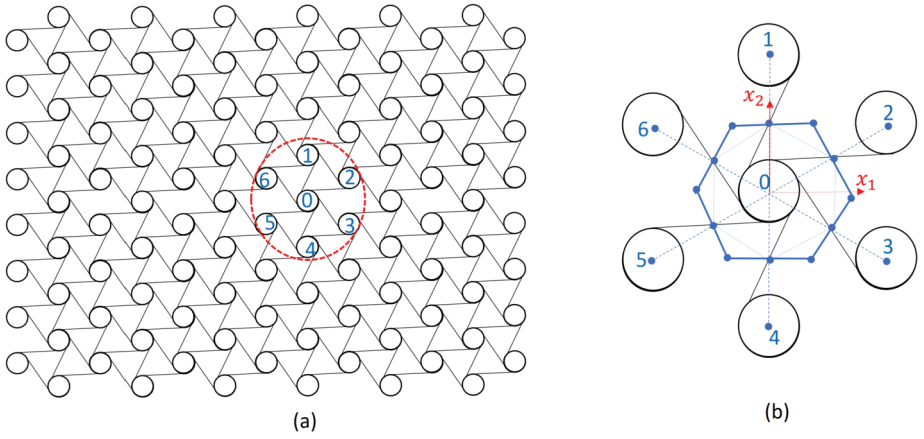

Fig. 5 The singum modeling of a chiral lattice: (a) the overall chiral lattice with a representative node highlighted and (b) the singum particle of Node 0 as a primitive cell

is perpendicular to the bond, a smaller hexagon is obtained as the dot line, which cannot seamlessly fill the space anymore. The bond length $2l_p^0 = 2\sqrt{L^2 - R^2}$. In the illustrated case, $L = 2R$ and $l_p^0 = \sqrt{3}R$. Although the singum model is general, this paper uses the configuration in Fig. 5 (b) as an example to demonstrate the results.

The Cauchy–Born rule cannot be directly applied due to two features: First, the rigid ring cannot contribute to deformation and only the bond is elastic; secondly, the equilibrium of the singum or the rotational unit 0 will be questionable due to the moment produced by the bonds which do not pass the center point. However, the similar procedure to Sect. 3 can be applied with two cases.

Case I: *Fix the rotational unit 0, apply a DG variation δd_{ij} on the singum as a continuum, and calculate the displacement variation and the force variation at each cutting point through Eqs. (13) and (21), respectively, which leads to the resultant moment δM on the rotational unit.*

In this case, an external moment of $-\delta M$ shall be applied to keep the equilibrium of the rotational unit 0 and fix it. Note that the force equilibrium is satisfied as each bond has another identical one in the opposite direction to balance the force, although they are not on the same line, which produces the moment.

Case II: *Fix the cutting points, apply a moment variation δM on the rotational unit, and calculate the force on each bond.*

Because each bond shares the same distance to the center, the force magnitude on the bond will be $\frac{\delta M}{6R}$.

The superposition of the two cases will meet the equilibrium and deformation requirement, and the resultant force variation at each cutting point will define the stress variation through Eq. (14) and thus the stiffness of the singum.

The geometry information is provided in Table 1. Notice that directional vectors of **n** and **m** are overlapped in the previous four lattices as all bonds pass the center of Node 0, so **m** is simply represented by **n**. However, in the chiral lattice, **m** denotes the directional norm of the cutting point referred to Node 0; whereas **n** represent the bond's directional norm.

Table 1 The geometric information for the singum of a chiral lattice (length normalized by R)

Items	bond 0-1	bond 0-2	bond 0-3	bond 0-4	bond 0-5	bond 0-6
Joint Point $\mathbf{p}^I$	(-0.866,0.5)	(0,1)	(0.866,0.5)	(0.866,-0.5)	(0,-1)	(-0.866,-0.5)
Cutting point $\mathbf{x}^I$	(0,2)	(1.732,1)	(1.732,-1)	(0,-2)	(-1.732,-1)	(-1.732,1)
$\mathbf{n}=\frac{\mathbf{x}^I-\mathbf{p}^I}{\lvert\mathbf{x}^I-\mathbf{p}^I\rvert}$	(0.5,0.866)	(1,0)	(0.5,-0.866)	(-0.5, -0.866)	(−1,0)	(-0.5, 0.866)
$\mathbf{m}=\frac{\mathbf{x}^I-\mathbf{0}}{\lvert\mathbf{x}^I-\mathbf{0}\rvert}$	(0,1)	(0.866,0.5)	(0.866,-0.5)	(0,-1)	(-0.866,-0.5)	(-0.866,0.5)

Now consider **Case I**. The displacement at each cutting point caused by δd_{ij} is $\delta u_j^I = x_i^I \delta d_{ij}$, and the force variation can be written as

$$\delta f_i^I = \frac{1}{2l_p^0}\frac{d(V_{,\lambda}n_i^I)}{dx_l^I}\delta x_l^I = \frac{1}{2l_p^0}\left[(V_{,\lambda\lambda}/l_p^0 - V_{,\lambda}/l_p)n_i^I n_l^I x_k^I + V_{,\lambda}/l_p \delta_{il} x_k^I\right]\delta d_{kl}. \tag{51}$$

Considering $|\mathbf{x}^I - \mathbf{0}| = \frac{2}{\sqrt{3}}l_p$, one can rewrite the above equation as:

$$\delta f_i^I = \frac{1}{\sqrt{3}l_p^0}\left[(V_{,\lambda\lambda}\lambda - V_{,\lambda})n_i^I n_l^I m_k^I + V_{,\lambda}\delta_{il} m_k^I\right]\delta d_{kl}. \tag{52}$$

The moment variation caused by the force variation of each bond is through the joint point $\mathbf{P}^I$, where $\mathbf{n}^I$ is perpendicular to $\mathbf{P}^I$. With the reference at Node 0, the moment variation is written as

$$\delta M^I = R n_i^I \delta f_i^I = \frac{1}{3}\left[(V_{,\lambda\lambda}\lambda - V_{,\lambda})n_l^I m_k^I + V_{,\lambda} n_l^I m_k^I\right]\delta d_{kl} = \frac{\lambda V_{,\lambda\lambda}}{3} n_l^I m_k^I \delta d_{kl}, \tag{53}$$

where $R = l_p^0/\sqrt{3}$ is used. Therefore, the total moment variation on the rotational unit is

$$\delta M = \sum_{I=1}^{6} \delta M^I = \sum_{I=1}^{6} \frac{\lambda V_{,\lambda\lambda}}{3} n_l^I m_k^I \delta d_{kl} \tag{54}$$

Now consider **Case II**. When the cutting points are fixed, applying δM on the rotational unit, the force variation on each bond is equal along the bond direction as follows

$$\delta f_i^I = -\frac{n_i^I}{6R}\sum_{J=1}^{6}\frac{\lambda V_{,\lambda\lambda}}{3} n_l^J m_k^J \delta d_{kl} = -\frac{n_i^I}{6\sqrt{3}l_p^0}\sum_{J=1}^{6}\lambda V_{,\lambda\lambda} n_l^J m_k^J \delta d_{kl}. \tag{55}$$

Therefore, the actual force variation on each bond is the superposition of the two cases in Eqs. (52) and (55) and the stress variation can be written as

$$\begin{aligned}\delta s_{ij} =& \frac{1}{V_s}\sum_{I=1}^{6}\left[x_i^I \delta F_j^I + x_k^I \delta d_{ki} F_j^I - x_i^I F_j^I \delta d_{kk}\right] \\ =& \frac{2}{3V_s}\sum_{I=1}^{6}\Big[(\lambda^2 V_{,\lambda\lambda} - \lambda V_{,\lambda})m_i^I n_j^I n_l^I m_k^I + \lambda V_{,\lambda} m_i^I m_k^I \delta_{jl} \\ & -\frac{1}{6}m_i^I n_j^I \sum_{J=1}^{6}\lambda^2 V_{,\lambda\lambda} n_l^J m_k^J\Big]\delta d_{kl}\end{aligned} \tag{56}$$

$$+\frac{\sqrt{3}}{3V_s}\sum_{I=1}^{6}\left[\lambda V_{,\lambda}(m_k^I n_j^I \delta_{il} - m_i^I n_j^I \delta_{kl})\right]\delta d_{kl},$$

where $V_s = 2\sqrt{3}L^2 = \frac{8}{\sqrt{3}}(l_p^0)^2$. Therefore, the stiffness tensor can be written as

$$\begin{aligned} C_{ijkl} =& \frac{2}{3V_s}\sum_{I=1}^{6}\left[\lambda^2 V_{,\lambda\lambda}\left(m_i^I n_j^I n_l^I m_k^I - \frac{1}{6}m_i^I n_j^I \sum_{J=1}^{6} n_l^J m_k^J\right)\right. \\ &\left. + \lambda V_{,\lambda}\left(m_i^I m_k^I \delta_{jl} + \frac{\sqrt{3}}{2}(m_k^I n_j^I \delta_{il} - m_i^I n_j^I \delta_{kl}) - m_i^I n_j^I n_l^I m_k^I\right)\right]. \end{aligned} \tag{57}$$

6.2 The Interpretation of the Matrix Form of the Stiffness

The stiffness tensor in Eq. (57) can be written in the generalized Voigt matrix form as:

$$\begin{aligned} \mathbf{C} = \frac{1}{4\lambda\sqrt{3}(l_p^0)^2}&\left[\lambda V_{,\lambda\lambda}\begin{pmatrix} 0.75 & -0.75 & 0.00 & 0.00 \\ -0.75 & 0.75 & 0.00 & 0.00 \\ 0.00 & 0.00 & 0.75 & 0.75 \\ 0.00 & 0.00 & 0.75 & 0.75 \end{pmatrix}\right. \\ &\left. + V_{,\lambda}\begin{pmatrix} 1.1250 & -2.6250 & 0.6495 & 0.6495 \\ -2.6250 & 1.1250 & -0.6495 & -0.6495 \\ 0.6495 & 1.9486 & 1.8750 & 1.8750 \\ -1.9486 & -0.6495 & 1.8750 & 1.8750 \end{pmatrix}\right]. \end{aligned} \tag{58}$$

Consider the chiral lattice shown in Fig. 5 with $R/L = 0.5$. When it is unstressed at $V_{,\lambda} = 0$, the lattice is instable for the rigid motion as $d_{11} = d_{22}$, which exhibits a negative Poisson's ratio of -1. Unlike the auxetic lattice in Fig. 3 with zero shear resistance, the chiral lattice exhibits a high shear modulus.

When a prestress exists with $V_{,\lambda} \neq 0$, the stiffness of the lattice is full and highly anisotropic without major symmetry. Given a uniaxial displacement controlled load d_{11}, the four stress components are different without minor symmetry either. Therefore, 16 independent elastic constants may be required to describe a general 2D lattice. Again, the equilibrium of the prestress is an issue, which will be discussed subsequently in the next section.

7 Remarks and Discussion

Five types of 2D lattices are demonstrated for singum modeling of the effective stiffness with the analytical formulations. When the material exhibits a lattice microstructure at the microscale and is used for structural applications, it can be treated as a homogeneous continuum. Considering the anisotropy and asymmetry of the stiffness tensor, the conventional elastic theory needs to be extended to accommodate the new features of lattice materials, which may not be found in nature but can be fabricated in the laboratory. The singum model can capture the physics and mechanics of lattice materials in a rigorous way.

7.1 The Balance of Mass, Momentum, and Strain Energy

As the singum construction is based on the WS cell of the lattice at the current configuration, the mass of a singum will remain constant as m_s due to the periodicity and the conversation of overall mass. The effective density can be defined as

$$\rho = \frac{m_s}{V_s} \tag{59}$$

and the mass variation of a singum caused by the DG variation δd_{ij} is always zero as

$$\delta m_s = \delta\rho V_s + \rho\delta V_s = 0 \quad \text{or} \quad \delta\rho = -\rho\delta d_{ii}. \tag{60}$$

The stress is defined through the equilibrium equation and stress boundary condition of Eqs. (6 - 8). The resultant force and moment on each singum has been required to be balanced, which is automatically satisfied for the lattice with central symmetry with the Cauchy–Born rule. For the auxetic and chiral lattices, the Cauchy–Born rule leads to the loss of the equilibrium in the resultant force and moment, respectively, and a secondary set of forces were superposed to make the conservation of momentum. Therefore, in absence of body force or distributed moment, the bond force variation on the lattice cutting points shall satisfy the equilibrium equations for both linear and angular momentum

$$\sum_{I=1}^{N} \delta\mathbf{f}^I = 0 \quad \text{and} \quad \sum_{I=1}^{N} \mathbf{x}^I \times \delta\mathbf{f}^I = 0 \tag{61}$$

and the stress variation on the continuum particle also shall satisfy

$$\sum_{I=1}^{N} L^I \mathbf{n}^I . \delta\mathbf{s} = 0 \quad \text{and} \quad \sum_{I=1}^{N} L^I \mathbf{x}^I \times (\mathbf{n}^I . \delta\mathbf{s}) = 0, \tag{62}$$

where σ^s is the average stress on the singum particle, so it is a constant tensor over the singum, and L^I is the edge length of singum corresponding to the Ith cutting point. For a closed polygon, the identity $\sum_{I=1}^{N} L^I \mathbf{n}^I = 0$ and $\delta\sigma^s_{ij} = \delta\sigma^s_{ji}$ can guarantee the above equation. In other words, when the lattice material exhibits zero distributed moment, the stress is symmetry for the equilibrium.

In addition, the equilibrium of the prestress is also an issue. For the central symmetric lattices or the honeycomb lattice, a prestress corresponding to $V_{,\lambda} \neq 0$ under the Cauchy–Born rule can always be self-balanced. However, a prestress corresponding to $V_{,\lambda} \neq 0$ for the auxetic and chiral lattices may produce a resultant force and moment on the singum node, respectively. If no effectively distributed body force or moment exists, such a prestress state of $V_{,\lambda} \neq 0$ can be nonphysical due to the loss of equilibrium. Instead, the compatibility and equilibrium condition can lead to different stretch ratios of λ^I for different bonds.

The elastic energy in the system due to the DG variation can be written in terms of the force and displacement in the lattice and the strain energy in the continuum singum particle, respectively, as

$$\delta W_s = \sum_{I=1}^{N} f^I_j \delta u^I_j = \sum_{I=1}^{N} f^I_j \delta d_{ij} x^I_i \quad \text{and} \quad \delta U_s = s_{ij}\delta d_{ij} V_s, \tag{63}$$

which are equivalent due to the definition of singum stress $s_{ij} = \sum_{I=1}^{N} f_j^I x_i^I / V_s$ in Eq. (10). Therefore, the elastic energy stored in the springs/bonds or lattice is the same as the strain energy in the singum particles or effective solid. Because the potential energy of the bonds is path-independent, the strain energy of the effective solid is also path-independent.

Overall, the mass, momentum, and elastic energy in the lattice are equivalent to those in the singum particle. As the elastic system of a lattice with a well-defined structure shall exhibit a specific, unique effective stiffness, the singum model provides the exact prediction, which has been verified by the numerical simulation of large lattice structures with boundary loading [45]. Note that when a lattice is instable in a certain deformation mode, it exhibits a zero or negative elastic modulus in that deformation mode. The singum predicts it as well.

In the literature, the strain energy equivalence between the lattices and the continuum has been used to homogenize the lattice and derive the effective elastic tensor [1, 27]. Based on the energy equivalence of Eq. (63), the singum model shall provide the same results as the strain energy equivalence when the prestress is not considered, because the effect of the configurational stress disappears. The only difference is that the singum model is a vectorial method instead of an energy method. Indeed, our recent paper showed the singum and energy methods provide the same results for example of granular lattices with central symmetry at $V_{,\lambda} = 0$ [45]. Here Ostoja-Starzewski also provided the same result in Eq. (2.23) of [27] as Eq. (19) of this paper. When prestress exists, the strain energy variation will be more complex and numerical methods can be used for energy method. However, they might not provide the exact solution as the singum model does. As d_{12} and d_{21} produce different stress states for some cases, but the strain energy has no way to differentiate d_{12} and d_{21} as only their mean value is used as strain. That is the reason why Berinskii [1] used the average of four terms to show the shear modulus. There is no way to use the classical strain energy in terms of symmetric strain to discover this problem of asymmetry and solve it. However, the vectorial method in the singum model directly works on the stress and DG with volume average, so that it can illustrate and solve the problem. The singum model indeed provides a simple, direct, and exact homogenization in Eqs. (8) and (11), which transfer the force and displacement of the bonds to the singum stress and strain by the Gauss theorem. Given a displacement variation, from the variations of the singum stress and strain, we can obtain the effective stiffness analytically and exactly.

7.2 Remarks About Anisotropy and Asymmetry of the Effective Elasticity of Lattices

The five types of lattices represent different features of elastic behavior of the lattice materials and may cover a large spectrum of lattice material behavior. Although the singum model is general and can be applicable to many new types of lattices and 2D or 3D, the following remarks are made from the five types of lattices, which can be expanded in future as well.

1. For the regular hexagonal lattice, it is isotropic and exhibits a Poisson's ratio at $\nu = 1/3$ in the unstressed state. Under the plane strain condition, $\nu = 1/4$. Classical elasticity and the Cauchy–Born rule can perfectly describe the problem.
2. For the regular hexagonal lattice, when a prestress exists, the compressive stress leads to the increase of the Poisson's ratio, and vice versa.
3. A honeycomb lattice is instable in the unstressed state with zero shear resistance and the Cauchy–Born rule is not applicable. When a tensile hydrostatic prestress exists in the bonds, it exhibits an isotropic elastic tensor. The Poisson's ratio $\nu = 1$ at the unstressed state and reduces with the tensile prestress.
4. When a lattice is unstressed in each bond, the major symmetry is satisfied. However, the prestress leads to configurational stresses, which changes the major symmetry and

increases the anisotropy of the stiffness tensor for unbalanced lattices with the singum node not at the center of the singum (Fig. 3) or the various bond lengths (Fig. 4).
5. The stiffness matrix obtained by the incremental DG shows the stability and rigid body motion of the lattice by the sign of the elastic constants and linear dependency of the stiffness matrix.
6. The auxetic lattice in Fig. 3 exhibits anisotropic elastic behavior and high negative Poisson's ratio and the limit in classical elasticity is not applicable. Moreover, d_{12} and d_{21} yield different shear stresses. The symmetry strain tensor cannot catch this asymmetric effect. Therefore, the singum strain d_{ij} is recommended to replace the classical strain tensor for this material.
7. When the bonds pass the singum node in Figs. 1, 2, and 4, a symmetric stress tensor is still sufficient to describe the constitutive relation. However, for an auxetic or chiral lattice (Figs. 3 and 5), an asymmetric stress tensor is required to describe the constitutive law.
8. For different lattices, different symmetry patterns exist. For the most general cases, 9 stress or DG components for 3D and 4 stress or DG components for 2D are required, so 81 and 16 elastic constants may exist for 3D or 2D lattices whose major symmetry is lost.

The singum model is not only applicable to the lattice material with linear elastic bonds, it can be used in granular materials, crystal lattices, among other materials with periodic microstructure and point-point interactions or potentials [41, 42, 45]. In classical elasticity, the prestress or residual stress in the material and structures were often addressed by the superposition. However, the singum model clearly shows its effects on the effective elastic tensor as well, which leads to nonlinear elastic behavior. Particularly, in geothermal or in outer space applications, the pressure may significantly change from the measurements in the laboratory settings, the singum model will enable the accurate prediction of the nonlinear, anisotropic and asymmetric elastic behavior.

7.3 Impacts to the Theory of Elasticity

In this paper, the 2D continuum is essentially formed by 1D bonds. Although the 1D bonds are assumed to be linear elastic in this paper, the 2D continuum is nonlinear elastic instead, due to the configurational stresses caused by the prestress on the area and shape variation of the singum. Therefore, the constitutive law can be very different from the classical elasticity for some special lattices. Because the tangential stiffness of a lattice can be explicitly predicted based on the microstructure and stress state, the nonlinear elastic problems can be solved by linearization of the stress-DG in an incremental way. For each step, the governing equation can be written as:

$$C_{ijkl} u_{l,ki}(\mathbf{x}) + b_j(\mathbf{x}) = 0, \tag{64}$$

where b_j is the body force and C_{ijkl} shall be undated with the current stress state and lattice configuration. Together with boundary conditions, a typical boundary value problem can be set up with the partial differential equation. Note that the order of the dummy indices shall be consistent when the symmetry does not exist; whereas classical elasticity is not sensitive to the order of ij or kl. Note that because the 2D continuum is nonlinear elastic, the principle of superposition in linear elasticity shall not be used. However, the energy conservation is still applicable because the energy is stored in the potential of the bonds.

For special lattices without symmetry, because the symmetry condition does not exist, the traditional compatibility of stress or strain tensors are not required anymore. However,

for a solid without any distributed moment, the shear stress shall be symmetric under the equilibrium condition, a new equilibrium condition shall be enforced as

$$C_{ijkl}u_{l,k} - C_{jikl}u_{l,k} = 0 \tag{65}$$

in solving the boundary value problem. When a distributed moment is prescribed, the above equation shall be revised accordingly to balance the distributed moment.

One misconception may exist for the stress by the rigid body motion. Consider the superposition principle in classical elasticity, a rigid body motion can be achieved by the superposition of $u_{i,j}$ and $-u_{j,i}$ in the infinitesimal deformation, which shall lead to a zero stress state, i.e. $C_{ijkl} - C_{ijlk} = 0$. Considering the symmetry of stress or $C_{ijkl} = C_{jikl}$, one can obtain the minor symmetry. This is also the reason why the symmetric strain is used in classical elasticity. However, in finite deformation, the superposition of $u_{i,j}$ and $-u_{j,i}$ cannot achieve the rigid body motion. This requirement is not necessary. Indeed, a certain shear DG of $u_{1,2}$ of $u_{2,1}$ requires different shear stresses in some lattices, $C_{ijkl} - C_{ijlk} \neq 0$ discloses the mechanics of those lattices, but is not against the physics that a rigid body motion exhibits the zero stress state.

Another misconception is that the lack of the major symmetry implies that the effective continuum does not have a strain potential and therefore can produce energy when deformed in closed loops in strain space [2]. This statement is correct to an infinitesimal strain cycle with linear elasticity, in which the Betti reciprocity and the superposition principles can be applied [2, 6]. However, for lattice-based materials, even though the linear elastic bonds are assumed, the effective elastic behavior is nonlinear. The singum model provides the exact prediction of the tangential elastic constants for the nonlinear elastic behavior, but the elastic conservative nature is still followed with the bonds due to the energy equivalence in Eq. (63) in spite of the loss of the major symmetry of the elastic tensor that is caused by the configuration stress of the existing forces. Therefore, the loss of the major symmetry does not mean the loss of the conservative nature of strain energy in the system for the finite deformation with nonlinear elastic behavior of the lattice-based materials.

Interestingly, the recently proposed odd elasticity [30] also uses DG in the constitutive modeling of the active, non-conservative solids, which exhibit the loss of major symmetry of the stiffness as well. However, there exist the following 3 distinctions from this paper:

1. The bond in the odd elasticity is not based on the pair potential, which lead to the transverse force that is perpendicular to the center-center line of the bond. The transverse force outputs work, causes the non-conservation of energy in a closed strain loop and the anti-symmetric part in the effective elastic tensor with $C^o_{ijmn} = -C^o_{mnij}$. However, this paper uses the pair potential that only produces force along the bonds, so that the strain energy is conservative and only depends on the starting and ending state. Note that the conservative nature does not guarantee the major symmetry unless linear infinitesimal strain is assumed.
2. The odd elasticity is still based on the linear superposition principle, in which the DG is decomposed into four modes, and each mode includes the combination of two DG components. For example, the rigid body motion is $u_{1,2} - u_{2,1}$. However, this paper considers the nonlinear elastic nature caused by dimension change from 1D linear elastic bonds to the 2D solid, and a given force in the system will produce configurational stress in the new stress state when another load is applied, so that the overall stress state cannot be the linear addition of the two individual stress states. Moreover, the rigid body motion of $u_{1,2} - u_{2,1}$ is limited to the infinitesimal deformation, which incurs cautions for energy harvesting applications of the odd elasticity.

3. The odd elasticity adopts a coarse-graining network to calculate the effective elastic tensor, which follows the standard procedure of simulating a ball-and-spring lattice to large-scale deformations [30]. However, this paper derives the effective elastic tensor based on the variational method of the stress and strain on the singum particle with an explicit form, which was verified by the large-scale simulation as well [45] and is the exact solution for a lattice with short-range pair potential.

Overall, the loss of major symmetry is caused by two distinct reasons between the odd elasticity and this paper: the non-conservative bonds for the odd elasticity versus the configurational stress for the present singum model, respectively. However, the singum model can also be extended to the non-conservative bonds by introducing the corresponding forces, such as the friction between balls for a granular lattice [45], which will be reported in future work.

7.4 Emerging Applications and Future Work of the Present Method

The singum model is particularly straightforward to investigate the stress and force transfer in the lattice-based structure and materials cross the length scale. Although the bonds are assumed to follow the harmonic potential in this paper, which is realistic to cellular lattices with linear elastic bonds, the present method can be extended to other lattice materials with different potential functions. Crystal lattices exhibit high diversities in the lattice structures [36] and atom dynamics with phase transitions under mechanical and temperature loading [9, 13, 28], the symmetry of the lattices evolves with the deformation. The extension of the singum model for elastic tensor of crystal lattices is underway [42]. The key difference is that the atomic interactions depend on the relative locations with the long range effects, while cellular lattices are formed by predefined bonds or links. Therefore, the singum may annihilate and reform during the phase transition of crystal lattices.

This paper focuses on 2D lattices and their in-plane elastic behavior. It can be extended to the out-of-plane elastic behavior for mono-layered crystal lattices [7, 31], in which the thickness of the lattice layer can be a controversial issue [8]. The same procedure can be applied to 3D lattices [42].

Given the stress at the macroscale, the singum model can predict the force in the bonds, and vice versa. Therefore, we can predict the nonlinear elastic behavior of the lattice materials. The stability and strength of the bonds will lead to the buckling, fracture, collapse, and damage of the material at the macroscale. Therefore, the present singum model and constitutive law lay a solid foundation for the inelastic behavior of the lattices as well.

8 Conclusions

The singum model has been applied to lattice metamaterials for prediction of the effective elasticity based on the stiffness of the lattice components with a linear elastic potential, in which the load is transferred through the lattice network represented by unit cells. A singum particle is introduced as the WS cell of the lattice to represent its behavior at the continuum level. The average stress and displacement gradient (DG) on the singum are defined as the singum stress and strain. The variational method is used to investigate the equilibrium of the singum, evaluate its averaged stress variation caused by a displacement variation, and thus derive the tangential stiffness analytically. Using the singum model in 5 lattices, one can make the following conclusions:

1. When central symmetry of the unit cell is satisfied, a single singum particle can represent the lattice and the Cauchy–Born rule provides the elastic tensor. Although most lattices exhibit anisotropic elasticity, a two-dimensional (2D) hexagonal lattice provides an isotropic elastic tensor in plane stress condition with a Poisson's ratio $\nu = 1/3$ and in plane strain condition with $\nu = 1/4$ if no prestress exists. Otherwise, the Poisson's ratio reduces with the tensile prestress and increases with a compressive prestress.

2. When the central symmetry of the unit cell is not satisfied, the primitive unit cell will contain more than one singums and the Cauchy–Born rule leads to the loss of equilibrium of the single singum. A secondary stress is induced to balance the singums. Due to the prestress, configurational stresses are induced, which changes the stiffness significantly.

3. For some special lattices with the bonds not passing singum's center, the angle between neighboring bonds not equal, due to the prestress, the same incremental d_{12} and d_{21} may lead to different stress variations, which lead to the loss of minor symmetry of the stiffness. Without the distributed moment, the stress shall be symmetric. Therefore, the loss of minor symmetry also leads to the loss of major symmetry.

4. The lattice elastic behavior is highly nonlinear even though the bonds are linear elastic. Given a stress state in a 2D lattice configuration, 4 stress and 4 strain components are required in the incremental constitutive relation, in which the tangential stiffness requires 16 elastic constants when minor or major symmetry does not exist. However, the strain energy is conservative following the potential of bonds.

Although only five 2D lattices are demonstrated, they cover some representative anisotropic and asymmetric elastic behavior with 8 remarks provided. It is straightforward to extend the model and related conclusions to 3D lattices.

Appendix A: Determination of the Force Transfer Matrix R

Consider a truss system of N bars, which connect to one singum node at one end with another end fixed by hinges as the cutting point. All bars are assumed to exhibit the same length and elastic constants for simplicity, and the number of the bars is large enough to make the truss system stable or indeterminate. When all the cutting points are fixed, given a force P_i on the singum node, the force transferred to the Ith bar can be written as

$$T_j^I = P_i R_{ij}^I, \tag{66}$$

which is along the bar with the direction from the singum node to the cutting point $\mathbf{n}^I$. Here, the conventional summation of double index notation is applied to the subscript with lower case symbols only.

Consider the force in each bar is given at $\mathbf{f}^I = \frac{V_\lambda n_i}{2l_p^0}$. Without the loss of any generality, set the origin $\mathbf{0}$ at the singum node and the cutting points are fixed at $\mathbf{x}^I$ $(I = 1, 2, \ldots, N)$ with $l_p = |\mathbf{x}^I| = \lambda l_p^0$, so $\mathbf{n}^I = \mathbf{x}^I / l_p$.

When all cutting points are fixed, a small variation of the singum node, $d\mathbf{x}$, will change the bond vectors into $\mathbf{x}^I - d\mathbf{x}$, which leads to a length change

$$dl^I = -n_i^I dx_i \tag{67}$$

and an orientational change

$$dn_i^I = \frac{n_i^I n_j^I - \delta_{ij}}{\lambda l_p^0} dx_j \tag{68}$$

for the Ith bonds. Note that $d\lambda^I = dl^I / l_p^0$.

The force variation for each bar can be obtained as

$$df_i^I = \frac{V_{,\lambda\lambda} n_i^I d\lambda^I + V_{,\lambda} dn_i^I}{2l_p^0} = \left[\frac{-V_{,\lambda\lambda} n_i^I n_j^I}{2l_p^{0\,2}} + \frac{V_{,\lambda}(n_i^I n_j^I - \delta_{ij})}{2\lambda l_p^{0\,2}} \right] dx_j, \tag{69}$$

which includes two parts: the first is caused by the length change and the second orientational change. The resultant force variation on the singum is

$$df_i = \sum_{I=1}^{N} df_i^I. \tag{70}$$

Then the force transfer matrix R_i^I can be determined by the classical displacement method with the following procedure in 3D case, which can be reduced to 2D case straightforwardly:

1. Given a unit displacement $\mathbf{d}_1 = (1, 0, 0)$ on the singum node, the resultant force on the singum is calculated by Eq. (70), which is a sum of N vectors in 3D, namely $\mathbf{P}_1 = \sum_{I=1}^{N} \mathbf{f}^{I1}$.
2. Similarly, given a unit displacement $\mathbf{d}_2 = (0, 1, 0)$ or $\mathbf{d}_3 = (0, 0, 1)$ on the singum node, the resultant force on the singum can also be calculated as $\mathbf{P}_2 = \sum_{I=1}^{N} \mathbf{f}^{I2}$ and $\mathbf{P}_3 = \sum_{I=1}^{N} \mathbf{f}^{I3}$.
3. Given any displacement $\mathbf{d} = (a, b, c)$, the resultant force will be written as $\mathbf{P} = a\mathbf{P}_1 + b\mathbf{P}_2 + c\mathbf{P}_3$.
4. Solve $a\mathbf{P}_1 + b\mathbf{P}_2 + c\mathbf{P}_3 = (-1, 0, 0)$ with three equations for a, b, c. Using $d\mathbf{x} = (a, b, c)$, one can calculate force variation of each bar by Eq. (69), which defines $R_{1j}^I = df_j^I$.
5. Similarly, solve $a\mathbf{P}_1 + b\mathbf{P}_2 + c\mathbf{P}_3 = (0, -1, 0)$ or $(0, 0, -1)$ with three equations for a, b, c. One can obtain R_{2j}^I or R_{3j}^I, respectively.

Therefore, R_{ij}^I, which shows the force for member I due to a unit force in x_i, can be obtained.

Appendix B: A Case Study of a Honeycomb Lattice Truss System

To demonstrate the accuracy of the singum model, a case study is presented for a honeycomb lattice with harmonic potential or linear spring bonds between neighboring nodes. A MATLAB program is developed to simulate the elastic behavior of the lattice for verification of the formulation in Sect. 3, which can be straightforwardly extended to other lattices. In the program, an array of nodes are automatically generated based on the given lattice with the number of unit cells in X and Y directions. The $X - Y$ coordinate origin is set up on the center of the lattice. When the lattice is undergone a deformation, the new coordinate $x - y$ shares the same origin but the coordinates of the nodes change. A list of neighbors for each node is detected with the corresponding bonds and saved for the force computation

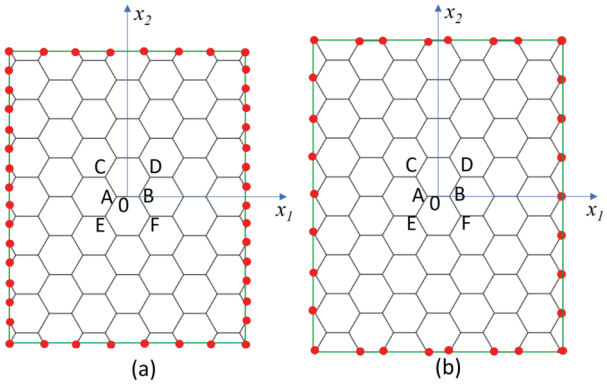

Fig. 6 The honeycomb lattice truss system with boundary: (a) at the mid-points of the bonds and (b) at the nodes

step. The mid-point of each bond is also important as the potential cutting point of singum surface.

Figure 6 schematically illustrates the honeycomb lattices. The boundary points can be selected by two cases. Figure 6(a) uses the mid-points of the bonds for the boundary; whereas Fig. 6(b) exhibits the boundary on the nodes. If the lattice approaches the infinite domain, the boundary selection produces negligible effects to the effective mechanical behavior. However, when finite unit cells are used, they may produce big differences with different convergence rates to the solution. Due to the periodicity of the singum, Fig. 6(a) provides a better performance and will be used in the study. The algorithm is structured and implemented as follows:

1. Initialize the simulation box by periodically extending the singum along x and y direction with N_x and N_y replications. The 4 sides of the box are made of loading bars as a boundary layer. The node on the boundary is connected to the loading bars by hinges. The initial bond length and force are at $r = 2l_p^0$ and $\mathbf{F}^I = 0$, respectively, so $\lambda = 1$.
2. Given a testing mode, such as tension or shearing, apply the corresponding uniform singum strain variation $\delta d_{ij} = 10^{-6}$ to the simulation box according to the Cauchy–Born (CB) rule. The new positions of all mid-points are updated through an affine transformation with δd_{ij}.
3. Calculate the coordinate of each node from the mid-points by the equilibrium of the node. The length change of each fiber and λ, and use the potential function $V(\lambda)$ to calculate the equilibrium bond forces. For each loading bar, collect all bond forces and calculate the effective stress vector on each bar in the deformed configuration. Using the effective stress vector on the 4 edges, one can obtain the stress variation caused by $\delta d_{ij} = 10^{-6}$ at $\lambda = 1$, and thus calculate the elastic tensor.
4. For any normalized fiber length or stretch ratio, namely λ^i, the coordinate of each node and the force in each bond can be calculated with the harmonic potential V in Eq. (5). Repeat Steps 2 and 3 to calculate the elastic tensor at λ^i. Therefore, the relation of elastic tensor and λ can be calculated.

Although the above calculation can guarantee the equilibrium of the internal nodes immediately with the periodic microstructure during the deformation, the result of the elastic tensor is affected by the cut-off for the boundary length but will quickly converge with the number of unit cell N_x and N_y.

On the contrary, if Fig. 6(b) is used directly to generate the new positions of nodes following the C-B rule, the equilibrium positions of the internal nodes will not be periodic

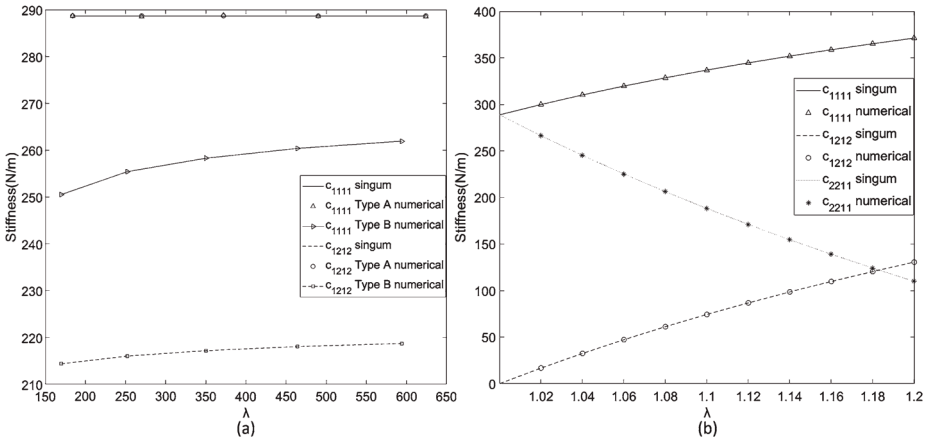

Fig. 7 Numerical simulation results of elastic tensors changing with different simulation scales and different boundary construction types(a) the comparison of the numerical simulation and the prediction of elastic tensors with different λ (b)

anymore, and a very large lattice is required to reach the convergent solution, which is demonstrated in Fig. 7(a).

As a numerical example, consider a lattice with $k = 1000N/m$, $l_p^0 = 1mm$, and $\lambda = 1$. Equation (33) provides $C_{1111} = C_{2211} = 288.6751$N/m and $C_{1212} = 0$N/m respectively. 7(a) shows the prediction of C_{1111} and C_{1122} changing with the increase of N_x or N_y (here we use $N_x = N_y$). Obviously, for type A lattice in Fig. 6(a), the simulation converges quickly with a few nodes. For instance, with only 184 nodes in total, the simulation results gave $C_{1111} =$ 288.6520N/m, compared to the prediction value from the singum model, the difference was only about 0.008%. However, for type B lattice in Fig. 6(b), the simulation converges much slower and requires more nodes to dilute the boundary effects as the displacement of nodes on top or bottom boundary does not follow the periodic distribution.

Using the type A lattice, we change the stretch ratio λ between 1.0 to 1.2, and show the comparison of the numerical simulation and the prediction of Eq. (33) in 7(b), which exhibit excellent agreement. Indeed, the singum model provides the exact solution for the lattice with the potential between short-range bonds.

Acknowledgements The author Yin thanks Professors Kefu Huang and Minzhong Wang for the fruitful discussion. The authors are also very grateful to Professor Glaucio Paulino for his encouragement and inspiration of this work and its extension to 3D origami-based lattices is underway.

Author contributions Yin wrote the main manuscript text, and Liu implement the numerical simulation to verify the formulation.

Funding This work is sponsored by the National Science Foundation IIP #1738802, IIP #1941244, CMMI #1762891, and U.S. Department of Agriculture NIFA #2021-67021-34201, whose support is gratefully acknowledged.

Declarations

Competing interests The authors declare no competing interests.

References

1. Berinskii, I.E.: In-plane elastic properties of auxetic multilattices. Smart Mater. Struct. **27**(7), 075012 (2018)
2. Bordiga, G., Piccolroaz, A., Bigoni, D.: A way to hypo-elastic artificial materials without a strain potential and displaying flutter instability. J. Mech. Phys. Solids **158**, 104665 (2022)
3. Cabras, L., Brun, M.: A class of auxetic three-dimensional lattices. J. Mech. Phys. Solids **91**, 56–72 (2016)
4. Chen, Y., Scarpa, F., Liu, Y., Leng, J.: Elasticity of anti-tetrachiral anisotropic lattices. Int. J. Solids Struct. **50**(6), 996–1004 (2013)
5. Cosserat, E., Cosserat, F.: Théorie des corps déformables. Librairie Scientifique A. Hermann et Fils (1909)
6. Coulais, C., Sounas, D., Alu, A.: Static non-reciprocity in mechanical metamaterials. Nature **542**(7642), 461–464 (2017)
7. Delfani, M., Shodja, H.: A large-deformation thin plate theory with application to one-atom-thick layers. J. Mech. Phys. Solids **87**, 65–85 (2016)
8. Delfani, M., Shodja, H., Ojaghnezhad, F.: Mechanics and morphology of single-walled carbon nanotubes: from graphene to the elastica. Philos. Mag. **93**(17), 2057–2088 (2013)
9. Ericksen, J.: On the symmetry of deformable crystals. Arch. Ration. Mech. Anal. **72**, 1–13 (1979)
10. Ericksen, J.: On the Cauchy–Born rule. Math. Mech. Solids **13**(3–4), 199–220 (2008)
11. Eringen, A.C.: Mechanics of micromorphic continua. In: Mechanics of Generalized Continua, pp. 18–35. Springer, Berlin (1968)
12. Eringen, A.C.: Microcontinuum Field Theories: I. Foundations and Solids. Springer, Berlin (2012)
13. Fadda, G., Zanzotto, G.: The arithmetic symmetry of monoatomic 2-nets. Acta Crystallogr., Sect. A, Found. Crystallogr. **56**(1), 36–48 (2000)
14. François, M.L., Chen, L., Coret, M.: Elasticity and symmetry of triangular lattice materials. Int. J. Solids Struct. **129**, 18–27 (2017)
15. Kole, S., Alexander, G.P., Ramaswamy, S., Maitra, A.: Active cholesterics: odder than odd elasticity (2020). ArXiv preprint arXiv:2012.14321
16. Lakes, R.: Experimental microelasticity of two porous solids. Int. J. Solids Struct. **22**(1), 55–63 (1986)
17. Lakes, R.: Foam structures with a negative Poisson's ratio. Science **235**, 1038–1041 (1987)
18. Lee, C., Wei, X., Kysar, J.W., Hone, J.: Measurement of the elastic properties and intrinsic strength of monolayer graphene. Science **321**(5887), 385–388 (2008)
19. Liu, K., Paulino, G.: Nonlinear mechanics of non-rigid origami: an efficient computational approach. Proc. R. Soc. A, Math. Phys. Eng. Sci. **473**(2206), 20170348 (2017)
20. Love, A.E.H.: A Treatise on the Mathematical Theory of Elasticity. Cambridge University Press, Cambridge (1906)
21. Mindlin, R.: Influence of couple-stresses on stress concentrations. Tech. Rep., New York (1962)
22. Mindlin, R.D.: Microstructure in linear elasticity. Tech. Rep., Columbia Univ. New York, Dept. of Civil Engineering and Engineering Mechanics (1963)
23. Mindlin, R.: Stress functions for a Cosserat continuum. Int. J. Solids Struct. **1**(3), 265–271 (1965)
24. Moosavian, H., Shodja, H.: Mindlin–Eringen anisotropic micromorphic elasticity and lattice dynamics representation. Philos. Mag. **100**(2), 157–193 (2020)
25. Mura, T.: Micromechanics of Defects in Solids. Springer, Netherlands (1987). https://doi.org/10.1007/978-94-009-3489-4
26. Nowacki, W.: Theory of Micropolar Elasticity. Springer, Berlin (1972)
27. Ostoja-Starzewski, M.: Lattice models in micromechanics. Appl. Mech. Rev. **55**(1), 35–60 (2002)
28. Pitteri, M.: On $\nu+1$-lattices. J. Elast. **15**, 3–25 (1985)
29. Saxena, K.K., Das, R., Calius, E.P.: Three decades of auxetics research- materials with negative Poisson's ratio: a review. Adv. Eng. Mater. **18**(11), 1847–1870 (2016)
30. Scheibner, C., Souslov, A., Banerjee, D., Surówka, P., Irvine, W., Vitelli, V.: Odd elasticity. Nat. Phys. **16**(4), 475–480 (2020)
31. Sfyris, D., Sfyris, G., Galiotis, C.: Curvature dependent surface energy for a free standing monolayer graphene: some closed form solutions of the non-linear theory. Int. J. Non-Linear Mech. **67**, 186–197 (2014)
32. Shodja, H.M., Ojaghnezhad, F., Etehadieh, A., Tabatabaei, M.: Elastic moduli tensors, ideal strength, and morphology of stanene based on an enhanced continuum model and first principles. Mech. Mater. **110**, 1–15 (2017)
33. Spadoni, A., Ruzzene, M.: Elasto-static micropolar behavior of a chiral auxetic lattice. J. Mech. Phys. Solids **60**(1), 156–171 (2012)

34. Tadmor, E.B., Miller, R.E.: Modeling Materials: Continuum, Atomistic and Multiscale Techniques. Cambridge University Press, Cambridge (2011)
35. Timoshenko, S., Goodier, J.N. (eds.): Theory of Elasticity. McGraw-Hill, New York (1951)
36. Wallace, D.C.: Thermodynamics of Crystals. Wiley, New York (1972)
37. Wang, M., Xu, B., Gao, C.: Recent general solutions in linear elasticity and their applications. Appl. Mech. Rev. **61**(3), 030803 (2008)
38. Wigner, E., Seitz, F.: On the constitution of metallic sodium. Phys. Rev. **43**(10), 804 (1933)
39. Willis, J.R.: Mechanics of composites. Ecole polytechnique, Département de mécanique (2002)
40. Yin, H.: A simplified continuum particle model bridging interatomic potentials and elasticity of solids. J. Eng. Mech. **148**(5), 04022017 (2022)
41. Yin, H.: Generalization of the singum model for the elasticity prediction of lattice metamaterials and composites. J. Eng. Mech. **149**(5), 04023023 (2023)
42. Yin, H.: Improved singum model based on finite deformation of crystals with the thermodynamic equation of state. J. Eng. Mech. **149**(4), 04023018 (2023)
43. Yin, H., Sun, L., Chen, J.: Magneto-elastic modeling of composites containing chain-structured magnetostrictive particles. J. Mech. Phys. Solids **54**(5), 975–1003 (2006)
44. Yin, H., Pao, F., Zadshir, M., Lou, J., Liu, C.: Tailoring thermoelastic constants of cellular and lattice materials with pre-stress for lightweight structure. U.S. Patent App. 17/935, 155 (2022)
45. Yin, H., Cui, J., Zadshir, M., Teka, L.: Effect of wrapping force on the effective elastic behavior of packed cylinders. J. Appl. Mech. **90**(3), 031003 (2023)
46. Zhang, W., Neville, R., Zhang, D., Scarpa, F., Wang, L., Lakes, R.: The two-dimensional elasticity of a chiral hinge lattice metamaterial. Int. J. Solids Struct. **141**, 254–263 (2018)